Depinning in a two-layer model of plastic flow

Pierre Le Doussal,[1] M. Cristina Marchetti,[2] and Kay Jörg Wiese[1]
[1]*Laboratoire de Physique Théorique–CNRS, Ecole Normale Supérieure, 24 rue Lhomond, 75005 Paris, France*
[2]*Department of Physics, Syracuse University, Syracuse, New York 13244, USA*
(Received 4 June 2008; published 2 December 2008)

We study a model of two layers, each consisting of a d-dimensional elastic object driven over a random substrate, and mutually interacting through a viscous coupling. For this model, the mean-field theory (i.e., a fully connected model) predicts a transition from elastic depinning to hysteretic plastic depinning as disorder or viscous coupling is increased. A functional renormalization group analysis shows that any small interlayer viscous coupling destabilizes the standard (decoupled) elastic depinning functional renormalization group fixed point for $d \leq 4$, while for $d > 4$ most aspects of the mean-field theory are recovered. A one-loop study at nonzero velocity indicates, for $d < 4$, coexistence of a moving state and a pinned state below the elastic depinning threshold, with hysteretic plastic depinning for periodic and nonperiodic driven layers. A two-loop analysis of quasistatics unveils the possibility of more subtle effects, including a new universality class for nonperiodic objects. We also study the model in $d=0$, i.e., two coupled particles, and show that hysteresis does not always exist as the periodic steady state with coupled layers can be dynamically unstable. It is also proved that stable pinned configurations remain dynamically stable in presence of a viscous coupling in any dimension d. Moreover, the layer model for periodic objects is stable to an infinitesimal commensurate density coupling. Our work shows that a careful study of attractors in phase space and their basin of attraction is necessary to obtain a firm conclusion for dimensions $d=1,2,3$.

DOI: 10.1103/PhysRevB.78.224201 PACS number(s): 62.20.fk, 83.50.−v, 83.60.Bc

I. INTRODUCTION

A. Overview

Nonequilibrium transitions from stuck to moving states underlie the physics of a wide range of phenomena,[1] from fracture and earthquake rupture[2–4] to flux flow in type-II superconductors[5,6] and sliding of charge density waves in metals.[7–10] The rich collective nonequilibrium dynamics of this broad range of phenomena can be modeled as an extended medium driven over quenched disorder. One can distinguish two main classes depending on whether the description allows or not for plastic deformations of the medium. Within each class one may restrict to microscopic overdamped dynamics or allow for more complicated, e.g., inertial, effects.

The first class of models, overdamped *elastic* media pulled by an applied force f, has been studied extensively. By definition, the driven medium can be deformed by disorder but is not allowed to tear, and topological defects are excluded, the only degrees of freedom being elastic deformations. The question of applicability of this model to realistic situations is still debated in the static case ($f=0$), and even more so in the driven dynamics. The general expectation is that such a model is relevant to describe real systems in some range of length scales, a range which becomes broad (and potentially infinite, depending on space dimension) in weak-disorder, strong-elasticity situations. Indeed one may conceive that, even if topological defects can be generated by the competition of elasticity, disorder and drive, they may remain bounded, and confined to shorter scales and thus unimportant for the effective large-scale description. This is known to happen in the statics, e.g., for interfaces in random ferromagnets. Even when topological defects are relevant at large scale, the elastic description may still apply at shorter scales. Hence the overdamped elastic model is a necessary first step to understand the collective dynamics in more complex situations. Many results were obtained for this model, although some questions remain open. At zero temperature ($T=0$) the elastic model exhibits a nonequilibrium phase transition from a pinned to a sliding state at a critical value f_c of the driving force, first studied in the context of charge density waves.[11,12] Starting from mean-field theory (MFT) (Ref. 13), an analogy with standard critical phenomena was developed, with the medium's mean velocity v acting as the order parameter, and a diverging correlation length.[1,13] A functional extension of usual renormalization group (RG) was developed to treat quenched disorder and obtain the roughness and dynamical exponents at the threshold $v=0^+$ to one-loop accuracy.[14,15] Extensions at nonzero v emphasized the differences with standard critical phenomena.[16] It was shown that a two-loop functional RG (FRG) approach is necessary to fully describe the difference between statics and $v=0^+$ quasi-static depinning[17–19] and to reach satisfactory agreement with numerical simulations.[20–22] Universality classes were identified, which are distinguished, for example, by the range of interactions or by the periodicity (or nonperiodicity) of the pinning forces. A key feature of the overdamped elastic model is that for one component displacements $N=1$, i.e., interfaces, the sliding state is unique, the $v(f)$ curve is single-valued, and no hysteresis can occur in the moving state at $v>0$. This property based on Middleton's theorem,[23] which also leads to simplifications[18] in the FRG description for $N=1$, is not expected to hold for $N>1$. As a result, the understanding of the $N>1$ depinning transition for e.g., lines or vortex lattices, is still not satisfactory despite some attempts.[24–26] Furthermore, there is a second type of universality class for depinning (e.g., anisotropic depinning) which does not obey the so-called statistical tilt symmetry (or rotation symmetry) and where nonlinear terms

become relevant [e.g., Kardar-Parisi-Zhang (KPZ)-type terms].[27] Despite efforts,[28,29] a complete theory for this class is still lacking, and even the value of the upper critical dimension is a matter of debate. The question of nonlinear terms may be of importance to experiments of contact line depinning and cracks.[30–32] Away from depinning, well into the uniformly sliding state at $v>0$, it was found that the dynamics can be surprisingly rich,[33] especially for $N>1$ component periodic objects.[34,35] New terms can be generated in the equation of motion, a linear convective term, a static random-force term, and a host of possible nonlinear, KPZ-type terms.[36–44] For $N>1$, a distinct, "moving glass" fixed point was found in the FRG, with persistence of transverse order and transverse pinning, leading to the prediction of a moving Bragg-glass and a moving smectic state.[38,42,43] In both states the flow is organized in staticlike channels, in a layered fashion. Extensions to correlated disorder was studied and a moving Bose-glass state was predicted.[45,46] Although clear evidence of these effects were found in numerics and experiments,[44] no systematic study of finite-size corrections was made. Since the simultaneous analytical treatment of all the terms allowed by symmetry within a FRG approach is a problem of formidable complexity,[43] even a fully consistent theory of the elastic flow at large velocity is still lacking. Hence the question of which moving state is stable in the thermodynamic limit is still open. Finally, once the elastic system is understood, one may hope to construct arguments for or against stability of the elastic flow to defects. These, however, are even more delicate than in the statics, where the stability of the Bragg glass was debated and the validity of the driven elastic model has only been assessed qualitatively.[42,43,47,48] Hence, as one can see, despite being well studied, the overdamped elastic model is still far from being understood. Extensions to include inertial effects and stress overshoots have also been considered,[49] but much work remains to be done. [Note that in the mean-field limit the stress-overshoot model and the model studied here (see below) are identical, aside from the fact that in the crack model nonperiodic disorder has been considered.]

There are many experimental situations where the elastic medium model seems insufficient and one needs to take into account plastic deformations as, e.g., topological defects in the medium. In a wide class of experiments strong disorder yields large deformations of the driven medium that make a strictly elastic model of the extended structure inapplicable.[50–53] In contrast, the medium tears as topological defects are constantly generated and healed by the interplay of drive, disorder and interactions.[53–60] At slow average flow rates the dynamics near depinning is spatially and temporally inhomogeneous, with coexistence of pinned and sliding degrees of freedom. The depinning transition may become discontinuous (first order), possibly with a macroscopic hysteresis and switching between pinned and sliding states.[61,62] Experiments on charge density waves show that varying the temperature leads to a transition from continuous depinning to hysteretic depinning with sharp switching between pinned and sliding states.[61] Whether such phase slip effects occur in the bulk or only at the contacts[63] remains to be clarified. Related slip effects or plastic behavior have been proposed to explain the complex dynamics of many other dissipative systems, including vortex arrays in type-II superconductors. Lorentz microscopy images of driven vortex arrays in irradiated thin films of niobium show vortex rivers flowing past each other at the boundaries of pinned regions of the lattice.[53] Scanning tunneling microscopy, which can resolve individual vortices at high density, also reveals the evolution of the vortex dynamics with disorder strength.[64] There too, there are edge contamination effects, and they may be responsible for the coexistence of a metastable disordered phase and a stable ordered phase.[65,66] It is clear that more work is needed to understand the rich dynamics of driven systems in experiments.

It was ubiquitously found in numerical studies of interacting particles driven on a random substrate at $T=0$ (away from the weak-disorder limit) that near the onset of mean sliding the motion occurs along filamentary channels or rivers that are determined by the spatial disorder of the random medium. Such channels are preferentially aligned along the direction of mean motion, but can exhibit large transverse excursions. At higher mean-flow rates the rivers coalesce into a more coherent structure that eventually results in a uniform flow. Hence the plastic flow takes, at a qualitative level, a variety of forms with increasing correlations: (i) filamentary flow with a single well-defined channel or several uncoupled channels[52,67–70] to coupled or synchronized channels, to a layered smectic type structure to a moving lattice which may or not still contain frozen or moving dislocations.[6,38,39,41–44] While one may hope that at large velocity, where the effective disorder is smaller, the flow is closer to the one described by an elastic model, it is clear that one needs to take into account plastic deformations to describe these various regimes.

The theoretical understanding of the dynamics of such plastic systems is much less developed than that of driven elastic media. It is not even clear how to characterize the various moving states which are observed by some order parameter, and to properly define steady states and their large-size limit. One can measure the distribution of time-averaged velocities $P(v)$ of the individual particles.[60] A nontrivial $P(v)$ exists for instance in the filamentary regime where some particles seem permanently pinned while others are moving along channels. In small systems with periodic boundary conditions a periodic steady state is observed near the threshold with a nontrivial $P(v)$. Whether this feature persists in the infinite system limit, and how it depends, e.g., on the geometry and aspect ratio of the sample, is not known. As was recently pointed out,[67] it is fruitful to apply tools and ideas from the theory of dynamical systems and chaos. It was found that upon increasing f, the system undergoes a transition from periodic to a fully chaotic flow with positive Lyapunov exponents and a nontrivial attractor. The dimension of this attractor, which is low, may also provide a tool to characterize the phases of plastic flow. These ideas remain to be explored, in particular whether the elastic flow could exhibit some chaotic regime. At larger drive, $P(v)$ becomes more peaked around a single velocity and some degree of spatial coherence in the phase across the layers may arise. Whether $P(v)$ eventually becomes a delta function in the large-size limit, and whether the phase-coherence lengths diverge or not, has not been systematically studied numeri-

cally. There has been some efforts to use numerical simulations to correlate the spatial and temporal structure of the dynamics with the shape of the macroscopic response,[60] for instance the *IV* characteristics due to flux flow in type-II superconductors. A number of mean-field models of driven extended systems with locally underdamped relaxation or phase slips have been proposed in the literature.[71–80] Whether or not these dynamical models exhibit truly collective behavior and universality in finite dimensions remains an open question which motivated this work, as discussed below. A model that attempts to describe filamentary flow away from mean field was proposed in Ref. 81.

B. Layered model

Given the difficulty in describing topological defects, a simpler approach consists in considering layers such that deformations within a layer are only elastic. Since the relative displacements between layers can be arbitrarily large, interlayer plastic deformations are allowed. Whether they occur or not depend on the interaction between the layers. This approach was successful to treat disorder in the statics, where it leads to solvable limits for e.g., the Bragg glass phase,[82,83] the decoupling transition for magnetically coupled superconductors.[84] It is also studied to describe interacting quantum systems such as the sliding Luttinger liquid.[85] Recently a similar strategy was applied to describe plastic flow and depinning (see Refs. 86 and 87 for a review), and coupling phenomena in the driven dynamics.[76] There it is even more natural since the flow naturally tends to be along layers (which can be channels) in the direction of the applied force. In one version of the model, introduced by one of us and collaborators,[80] it the layers are only *viscously* coupled in at least one of the directions transverse to the mean motion. Although this is a much simplified version of plastic flow, for instance there are no convective terms in the equation of motion, it is motivated by the moving smectic phase in driven vortex lattices mentioned above. It incorporates elastic responses to compressional deformations and allows for local slips of neighboring degrees of freedom due to shear deformations. It is also relevant to experiments on driven superconducting vortices in narrow channels and other controlled geometries.[88–92] One possible realization is a layered (e.g., high T_c) superconductor when the vortices are aligned with the magnetic field within the Cu_2O, *ab*-plane layers and move along these layers under a *c*-axis current. In the limit where the intrinsic pinning potential from the Cu_2O planes is strong compared to the weak isotropic disorder from point impurities, the vortex dynamics may be modeled in terms of $2d$ elastic layers or "channels" coupled viscously along the *c* axis. The fact that only the viscous coupling between layers is retained makes it more tractable. It is expected to be valid in situations where the commensurate density-density interlayer interaction, studied in Ref. 76, which couples the displacements in each layer, can be neglected. We wish to stress that the layered model studied here is inspired by the behavior of the driven system well above depinning and caution should be used in applying it to the regime of filamentary flow near depinning. One expects that the dynamics in this region be described by a nontrivial distribution of time-averaged velocities $P(v)$, while our model exhibits a uniform v, as appropriate at large drives.

The general case can be defined as follows. Consider a $d=d_\parallel+d_\perp$-dimensional medium composed of elastic $d_\parallel$-dimensional channels coupled via viscous interactions in the remaining $d_\perp$ directions. The medium is driven by a uniform force $\mathbf{f}$ applied along one of the directions in the $d_\parallel$-dimensional channels. Here we only consider the dynamics of a scalar displacement field $u(\mathbf{r}_\parallel,\mathbf{r}_\perp,t)$ describing deformations in the direction of the driving force at position $\mathbf{r}=(\mathbf{r}_\parallel,\mathbf{r}_\perp)$, with $\mathbf{r}$, $\mathbf{r}_\parallel$ and $\mathbf{r}_\perp$ vectors in d, $d_\parallel$ and $d_\perp$ dimensions, respectively. To index the channels one discretizes spatial coordinates in the direction normal to the layers ($\mathbf{r}_\perp \to \mathbf{r}_n$, where $\mathbf{r}_n$ denotes the nth layer) and let $\mathbf{r}_\parallel \equiv x$. The dynamics of the displacement $u_n(x,t)$ of each degree of freedom is governed by the equation

$$\gamma \partial_t u_n(x) = \int_{x'} K(x-x')[u_n(x)-u_n(x')] + \sum_{n=1}^{M} \eta_{n,m}[\dot{u}_m(x)-\dot{u}_n(x)] + f + F_n(u_n(x),x). \tag{1.1}$$

This is the M-layer model. Among the various universality classes of disorder, the one of most interest here is the random periodic class where the pinning force has the form

$$F_n(u_n,x) = h_n^i Y(u_n(x)-\beta_n^i), \tag{1.2}$$

with $Y(u)$ a periodic function. The pinning strengths h_n^i are independent random variables distributed with probability $\rho(h_n^i)$ and β_n^i are random phases uniformly and independently distributed in [0,1). This models the dynamics of driven periodic media such as vortex lattices, charge density waves, or Wigner crystals. In these systems substrate impurities couple to the density of the lattice which, in the absence of in-layer topological defects, has the periodicity of the ordered lattice. As a result, the pinning force contains periodic components at all reciprocal lattice vectors.[5,93] In the bare model one can retain the lowest Fourier components only, since as is well known from FRG studies of statics and depinning, all Fourier components are generated by coarse-graining and should be included to describe the properly renormalized disorder correlator. Such a correlator develops cusplike singularities at large scales that control the dynamics. The other type of disorder, the nonperiodic or random-manifold class, which at the elastic depinning was shown to give rise to a single universality class encompassing both random bond (i.e., short-ranged) and random field (i.e., long-ranged) disorder, will also be studied. This is done by choosing a nonperiodic correlator for the random forces $F_n(u,x)$. Physical realizations are less obvious since the above velocity coupling is local in x space only while a realistic coupling, e.g., between two directed polymers would also depend on the field u. Two possible realizations are the following: (i) manifolds with internal disorder as studied in Refs. 94 and 95 and (ii) periodic systems for which the correlation length of the disorder r_f is small compared to the lattice spacing a. Then the two

scales for pinning, the Larkin length R_c and R_a for the decay of translational order, can be very different and it is known that for scales $R_c \ll L \ll R_a$ all harmonics of the disorder correlator are important and the system behaves effectively as a random manifold within this range of scales.[5,35,96] Hence, below we also consider the nonperiodic or random-manifold model and discuss the different behaviors in the two cases.

C. Aim and outline of the paper: Two-layer model

The layered model (1.1) with viscous couplings was proposed as a generic coarse-grained model representative of a class of dissipative driven systems with strong disorder that encompasses many of the models considered in the literature. It was solved within mean-field theory and was shown to predict a qualitative change from continuous to discontinuous and hysteretic dynamics as a function of disorder strength, consistent with experimental observations in a variety of systems.[80] It has also been studied numerically in finite dimensions. The numerical studies show evidence of hysteresis in $2+1$ dimensions above a critical value of the interlayer coupling. Hysteresis was not clearly evident, however, in $1+1$ dimensions nor for the two-layer model studied below, although it could also not be conclusively ruled out on the basis of finite-size scaling.[97]

The aim of this paper is to go beyond the mean-field treatment of model (1.1) and explore using functional RG whether hysteretic dynamics also occurs and whether universal features emerge in low dimensions where one usually does not expect the mean-field approximation to be accurate. Since generalization to M layers is straightforward and not expected to bring important qualitative changes, we study in detail the technically simpler case of two viscously coupled layers $M=2$. We start by recalling in Sec. II the main features of the mean-field solution so as to provide a basis for comparison. In Sec. III we study the $M=2$ model first by direct perturbation theory and next using one-loop FRG. We prove that the elastic single-layer (i.e., decoupled layer) quasistatic $v=0^+$ depinning fixed point is *always unstable* to a small viscous interlayer coupling. A partial one-loop analysis at $v>0$ shows the generic coexistence of a pinned and a moving state below the single-layer depinning threshold. The resulting $v(f)$ curves show similarities with the mean-field ones and in some regimes the agreement can even be made quantitative. We estimate the velocity v_c at which the $v(f)$ curve becomes vertical (and a jump may occur in the fixed force ensemble). A key feature of the one-loop study is that the interlayer viscous coupling γ_{12} is *not corrected* by disorder. To determine whether this is maintained to higher order, we carry in Sec. IV the FRG to two loops, near the uncoupled elastic quasistatic depinning. The analysis gives a strong correction as compared to one loop in the nonperiodic class, i.e., random manifolds, with a new universality class for plastic depinning whose z exponent is computed in Sec. IV B. The analysis in the periodic case is quite subtle and presented in Sec. IV C. Finally, to get a better understanding of possible behaviors and of the connection between dynamical hysteresis and attractors in phase space in simpler cases, we study in Sec. V two $d=0$ toy models of two viscously coupled particles on, respectively, a smooth (Sec. V A) and a discontinuous (Sec. V B) force landscape. Finally, in Sec. V C the main results are summarized, and extensions and future directions discussed. In particular, it is proved that a small interlayer commensurate coupling is irrelevant at depinning. Since such a term is always present in real systems, this shows that the viscous model is consistent. Appendixes A and B contain the details of the two-loop calculation and a proof that stable static configurations where decoupled layers are independently pinned remain dynamically stable in presence of the interlayer viscous coupling.

Let us now define the two-layer model studied here, and fix notations. We consider the overdamped dynamics of two layers coupled by a viscous coupling in a random potential. Each layer is an elastic system parametrized by a one-component ($N=1$) displacement field $u^i(x)$, also denoted u^i_x, for $i=1,2$, or $u^i_{x,t}$ to indicate explicitly the dependence on time. The equation of motion of one layer is

$$\gamma_0 \dot{u}^1_{x,t} = \eta_0(\dot{u}^2_{x,t} - \dot{u}^1_{x,t}) + c\nabla^2 u^1_{x,t} + F^1(u^1_{x,t}) + f, \qquad (1.3)$$

where γ_0 is the in-layer friction coefficient. Hence, in addition to elastic intralayer restoring forces (elastic coefficient c) and the quenched random pinning force, one layer is also pulled by the other layer through a velocity (or viscous) coupling η_0. Here we focus on the case of uncorrelated disorder in each layer and denote the second cumulant of the pinning forces by

$$\overline{F^i(x,u)F^j(x',u')} = \delta^{ij}\delta^d(x-x')\Delta_0(u-u'). \qquad (1.4)$$

The equation of motion for the system of two layers driven by an external force f can then be written as

$$\begin{pmatrix} \gamma_{11} & \gamma_{12} \\ \gamma_{12} & \gamma_{22} \end{pmatrix} \frac{\mathrm{d}}{\mathrm{d}t} \begin{pmatrix} u^1_{x,t} \\ u^2_{x,t} \end{pmatrix} = c\nabla^2 \begin{pmatrix} u^1_{x,t} \\ u^2_{x,t} \end{pmatrix} + \begin{pmatrix} F^1(x,u^1_{xt}) + f \\ F^2(x,u^2_{xt}) + f \end{pmatrix}. \qquad (1.5)$$

The bare values for the friction matrix are

$$\gamma_{11} = \gamma_{22} = \gamma_0 + \eta_0, \qquad (1.6)$$

$$\gamma_{12} = -\eta_0. \qquad (1.7)$$

II. MEAN-FIELD THEORY

To set up the mean-field theory for the multilayered model, it is convenient to discretize space in both the transverse and longitudinal directions, using integer vectors ℓ, m for the $d_\parallel$-dimensional intralayer index. The local displacement along the direction of motion at time t is $u^i_\ell(t)$, with $i=1,\ldots,M$ as the layer index and $\ell=1,\ldots,N$ labeling the degrees of freedom within each layer. Its dynamics is governed by the equation (in this section we drop the subscript "0" on the bare frictions)

$$\gamma \dot{u}^i_\ell(t) = \sum_m K_{\ell m}[u^i_m(t) - u^i_\ell(t)] + \sum_j \eta_{ij}[\dot{u}^j_\ell(t) - \dot{u}^i_\ell(t)] + f + h^i_\ell Y(u^i_\ell(t) - \beta^i_\ell), \qquad (2.1)$$

where $Y(u)=Y(u+n)$ is a periodic function and $K_{\ell m}$ and η_{ij}

have constant values c and η, respectively, for nearest-neighbor pairs and vanish otherwise. The random pinning strengths h_ℓ^i are chosen independently with probability distribution $\rho(h_\ell^i)$ and the random phases β_ℓ^i are distributed uniformly and independently in $[0,1)$.

A. Fully connected mean-field theory

One mean-field approximation is obtained by assuming that all sites are coupled with uniform strength, both within each layer and across the layers, i.e., $K_{\ell m}=c/N$ for all ℓ and m and $\eta_{ij}=\eta/M$ for all i and j. The mean displacement and velocity are given by

$$\bar{u}(t)=\frac{1}{NM}\sum_{\ell}\sum_{i}u_\ell^i(t), \tag{2.2}$$

$$v=\frac{1}{NM}\sum_{\ell}\sum_{i}\dot{u}_\ell^i(t), \tag{2.3}$$

and we look for solutions moving with a uniform velocity so that (up to a choice of the origin of time)

$$\bar{u}(t)=vt. \tag{2.4}$$

Since the displacements are coupled only through the mean fields, they can be indexed by their disorder parameters β and h, rather than by the spatial indices ℓ, i, i.e., $u_\ell^i(t)\rightarrow u(t;\beta,h)$. The mean-field dynamics is governed by the equation

$$(\gamma+\eta)\dot{u}(t;\beta,h)=c(vt-u)+f+\eta v+hY(u-\beta) \tag{2.5}$$

that must be solved with the self-consistency condition that determines the mean field,

$$\langle u(t;\beta,h)-vt\rangle_{\beta,h}=0, \tag{2.6}$$

where $\langle\ldots\rangle_{\beta,h}=\int_0^1 d\beta\int dh\ldots\rho(h)$ denotes the average over disorder.

The long-time steady-state solution to Eq. (2.5) can be written as

$$u(t;\beta,h)=vt+\hat{u}, \tag{2.7}$$

with

$$(\gamma+\eta)\dot{\hat{u}}=-c\hat{u}+f-\gamma v+hY(\hat{u}+vt-\beta), \tag{2.8}$$

to be solved with the condition $\langle\hat{u}\rangle_{\beta,h}=0$. It is apparent from Eq. (2.8) that $\hat{u}$ is a periodic function of time with period $1/v$ and depends on time and phase β only through the combination $\hat{u}=\hat{u}(t-v/\beta;h)$. This will allow us to carry out the average over β by averaging over time.

We display below the solution for a parabolic scalloped pinning potential, corresponding to a piecewise linear pinning force with jumps of size h at the boundaries of each period,

$$Y(u)=n+\frac{1}{2}-u,\quad n\le u\le n+1, \tag{2.9}$$

with n as an integer. The mean-field Eq. (2.5) is formally identical to the mean-field equation for a purely elastic medium, with friction coefficient $\Gamma=\gamma+\eta$ and an effective drive $F=f+\eta v$. The solution of the mean-field equation for a scalloped pinning potential and $\eta=0$ was obtained by Narayan and Fisher[14] and is easily adapted to our case. The solution for finite η is described in Refs. 80 and 87 and will be summarized here for completeness.

The pinning force has a jump discontinuity h at the end of each period. The displacement $\hat{u}$ is continuous across neighboring periods, but the local velocity $\dot{\hat{u}}$ has jumps of size h/Γ at t_J+n/v. The solution of Eq. (2.8) for $t_J(\beta)+n/v\le t\le t_J(\beta)+(n+1)/v$ is

$$\hat{u}=Ae^{-\lambda t}+\frac{h(\beta-vt)+F+h(n+1/2)}{\Gamma\lambda}-\frac{cv}{\Gamma\lambda^2}, \tag{2.10}$$

where $\lambda=(c+h)/\Gamma$ and $t_J(\beta)$ is the "jump time." The constant $A(\beta)$ and the jump time $t_J(\beta)$ are determined by requiring

$$\hat{u}(t=t_J+n/v)=n+\beta, \tag{2.11}$$

$$\hat{u}(t=t_J+(n+1)/v)=n+1+\beta. \tag{2.12}$$

It is important to appreciate a crucial difference between the mean-field theory of the purely viscous model ($c=0$ or $d_\parallel=0$) discussed in Refs. 77 and 78 and the mean-field theory of the model considered here that includes additional elastic couplings within the channels. In the purely viscous case, each degree of freedom is coupled only to the local velocities (which exert an additional effective driving force) and can slide with its own period. In contrast, when $c\neq 0$ each degree of freedom couples to the average displacements via a spring-type interaction that forces all periods to be the same, independent of h.

After inserting A and t_J obtained from the solution of Eqs. (2.11) and (2.12) in Eq. (2.10), it is straightforward to impose the self-consistency condition as

$$\langle\hat{u}(t-\beta/v;h)\rangle_{\beta,h}=v\left\langle\int_{t_J+n/v}^{t_J+(n+1)/v}dt\hat{u}(t-\beta/v;h)\right\rangle_h=0. \tag{2.13}$$

This yields an implicit solution for the mean velocity as

$$F(v)=f(v)+\eta v=f_c+\Gamma v[1-M(c)]+\left\langle\frac{h^2}{(c+h)}\frac{1}{e^{\lambda/v}-1}\right\rangle_h, \tag{2.14}$$

with f_c as the threshold force for the onset of uniform sliding,

$$f_c=\left\langle\frac{h^2}{2(c+h)}\right\rangle_h, \tag{2.15}$$

and

$$M(c)=\left\langle\frac{h^2}{(c+h)^2}\right\rangle_h. \tag{2.16}$$

The threshold force depends only on the elastic coupling c, but not on the viscous coupling η. This follows because in mean field the viscous coupling becomes effective only when

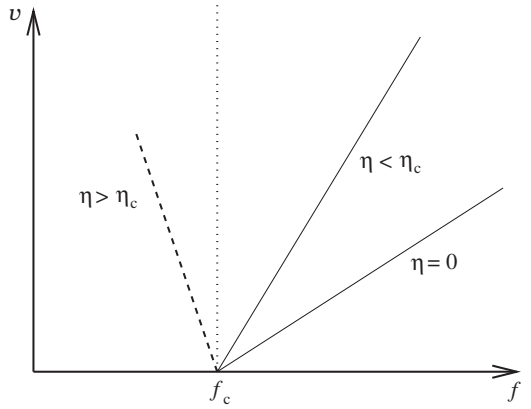

FIG. 1. The mean-field velocity $v(f)$ as a function of f near threshold, as given by Eq. (2.17). The slope of the linear function diverges at $\eta=\eta_c(c)$ and is negative for $\eta>\eta_c(c)$.

the system is moving as a whole, while away from mean field one expects additional fluctuation effects.

Near threshold the term on the second line of Eq. (2.14) gives contributions of order $\sim e^{-1/v}$ and can be neglected. It is then easy to invert Eq. (2.14) to obtain $v(f)$, with the result

$$v(f) \sim \frac{(f-f_c)^{\beta_{\mathrm{MF}}}}{\gamma-(\gamma+\eta)M(c)}. \tag{2.17}$$

The mean velocity vanishes linearly for $f\to f_c^+$, with a mean-field (MF) exponent $\beta_{\mathrm{MF}}=1$ which is generic for discontinuous pinning forces.[14] When $\eta=0$ the slope of the linear curve is always positive as $M(c)<1$. The slope diverges, however, at a critical value of η,

$$\eta_c(c) = \gamma\left[\frac{1}{M(c)}-1\right], \tag{2.18}$$

and becomes negative for $\eta>\eta_c$, as shown in Fig. 1. For $\eta>\eta_c(c)$ the velocity curve is multivalued, yielding hysteretic behavior.

The phase diagram and typical velocity-force curves are shown in Figs. 2 and 3 for $\rho(h)=\delta(h-h_0)$. The finite long-time elasticity ($c\neq 0$) guarantees that the behavior is *independent of the shape of the pinning-force distribution* $\rho(h)$. The phase diagram for $\rho(h)=e^{-h}$ was shown in Ref. 80 and has the same form as the one shown here. The point (η_c,f_c) is a *tricritical point* separating single-valued from multivalued velocity curves. For $\eta<\eta_c$, a continuous depinning transition at f_c separates a pinned state from a sliding state with *unique* velocity. A question addressed below is whether η_c remains nonzero in finite dimension and if so, whether the depinning transition for $\eta<\eta_c$ is in the same universality class as the depinning of an elastic medium ($\eta=0$).[13]

In our mean-field example, the linear response diverges at η_c as $v(\eta=\eta_c)\sim 1/\ln(f-f_c)$. For $\eta>\eta_c$ the solution is multivalued. In this case when the force is ramped up from zero the system depins at $f_c^>=f_c$. When the force is decreased from a value above f_c the system gets stuck at the lower value $f_c^<$, yielding hysteretic $v(f)$ curves.

For $\eta>\eta_c$ the mean velocity has a jump discontinuity. The value v_c of this jump is given by the solution of

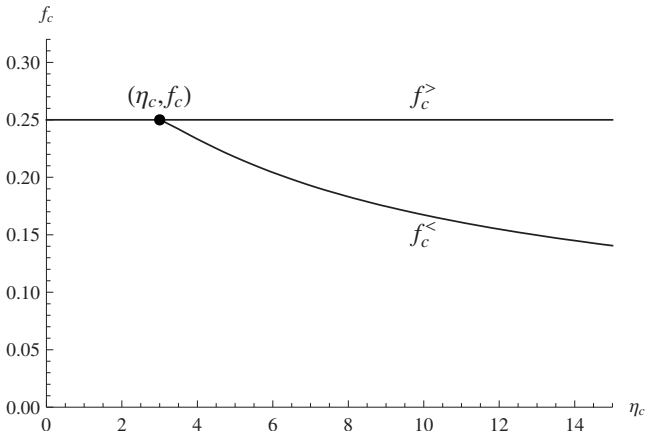

FIG. 2. Phase diagram obtained from the fully connected mean-field solution for $\rho(h)=\delta(h-1)$, for $\gamma=1$ and $c=1$, corresponding to $\eta_c=3$. There is a critical point at (η_c,f_c) separating continuous from discontinuous depinning.

$$\left(\frac{\partial f(v)}{\partial v}\right)_{v=v_c}=0, \tag{2.19}$$

where $f(v)$ is given by Eq. (2.14). An explicit solution for the jump v_c can be obtained for the case of a sharp disorder distribution $\rho(h)=\delta(h-h_0)$. In this case condition (2.19) for the jump becomes

$$\frac{\eta-\eta_c}{\gamma+\eta}=\frac{(\lambda/v)^2}{4\sinh^2(\lambda/(2v))}. \tag{2.20}$$

For $\eta\gg\gamma,\eta_c$ this gives

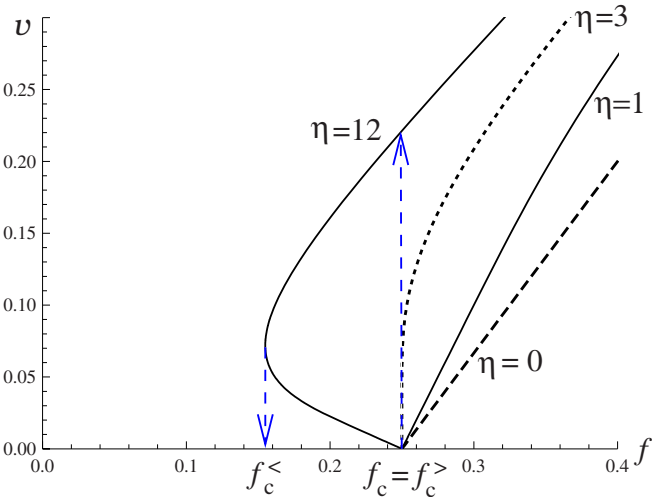

FIG. 3. (Color online) Typical velocity-force curves obtained from the fully connected mean-field solution for $\rho(h)=\delta(h-1)$, $c=1$ and $\eta_c=3$. For $\eta=0$ (dashed curve) and $\eta=1$ (solid line) the system depins continuously at f_c. At $\eta=\eta_c=3$ (dotted line) the slope diverges at threshold. For $\eta=12$ (solid line) the velocity-force curve is multivalued. This corresponds to a hysteretic depinning transition as the system depins at $f_c^>$ when the force is ramped up from zero and repins at the lower value $f_c^<$ when the force is ramped down from the sliding state.

$$v_c \approx \frac{c+h_0}{2\sqrt{3}\eta}\sqrt{\frac{\eta}{\gamma+\eta_c}}. \quad (2.21)$$

Finally, we note that the mean-field theory for a smooth periodic pinning potential gives qualitatively the same phase diagram, although with mean-field exponent $\beta_{\rm MF}=1/2$.

The fully connected mean-field theory discussed here for the layered visco-elastic model is formally identical to the mean-field limit of a model of crack propagation with stress overshoot studied by Schwarz and Fisher,[71,72,98] although the crack model contains random force disorder instead of the periodic disorder considered here.[86,87]

B. Self-consistent single-layer approximation

An alternative "partial" mean-field approximation treats only one direction of space using mean field and reduces the problem to an effective single-layer model. It is obtained by assuming uniform, i.e., infinite-range couplings of strength $\eta_{ij}=\eta/M$ across the layers for each in-layer site ℓ. The corresponding mean field is given by

$$v_\ell = \frac{1}{M}\sum_i \dot{u}^i_\ell(t). \quad (2.22)$$

In the thermodynamic limit of an infinite number of layers, assuming the system is self-averaging, the mean field v_ℓ will not depend on ℓ and this label can be dropped. The mean-field dynamics is then described by the equation

$$(\gamma+\eta)\dot{u}^i_\ell(t) = \sum_m K_{\ell m}[u^i_m(t)-u^i_\ell(t)] + f+\eta v + h^i_\ell Y(u^i_\ell(t)-\beta^i_\ell), \quad (2.23)$$

which must be solved with the condition $\langle \dot{u}^i_\ell\rangle_{\beta,h}=v$. It is illuminating to rewrite Eq. (2.23) by replacing the discrete in-layer index ℓ by the original continuum variable x,

$$(\gamma+\eta)\dot{u}^i_{x,t} = c\nabla^2 u^i_{x,t} + f+\eta v + h^i_x Y(u^i_{x,t}-\beta^i_x), \quad (2.24)$$

to be solved with the self-consistency condition $\frac{1}{M}\Sigma_i \dot{u}^i_{x,t}=v$. It is apparent that Eq. (2.24) describes the dynamics of M identical elastic layers coupled only through the mean field v. Each layer is a dissipative elastic medium of friction $\Gamma=\gamma+\eta$, driven by a force $F=f+\eta v$. For $\eta=0$ the layers are decoupled, with $\Gamma=\gamma$ and $F=f$. The velocity-force curve $v_{\rm sl}(f)$ of one decoupled layer has been studied in detail.[13,14,16,45,99,100] Each layer is pinned with $v=0$ for $f<f_c$. It depins at $f=f_c$ and slides for $f>f_c$ with mean velocity $v_{\rm sl}(f)=\mathcal{G}(f)/\gamma$, and $\mathcal{G}(f)\sim(f-f_c)^\beta$ as $f\to f_c^+$ and $\beta<1$ a critical exponent that depends only on the system's dimensionality. It is clear from the form of Eq. (2.23) that the velocity-force characteristic of the coupled layers has the same functional form as that of an individual layer, with the replacement $f\to F$, i.e, $v(F)=\mathcal{G}(F)/\Gamma$. A sketch of this velocity-force characteristic is shown in Fig. 4. The velocity-force characteristic $v(f)$ of the coupled layers can then be obtained simply by performing a shift in the independent variable in the known result for a single layer. The result is shown in Fig. 5. Near threshold $v(f)\sim(f+\eta v-f_c)^\beta$, with $\beta=1-(4-d_\parallel)/6+\mathcal{O}[(4-d_\parallel)^2]<1$ and $v(f)$ will be multivalued for every finite value of η, yielding a hysteretic depinning transition.[80] The hysteresis for any $\eta>0$, for $d<4$, obtained here in the approximation of a global transverse coupling, will be confirmed below within a one-loop FRG analysis which incorporates interlayer fluctuations neglected here. In both cases it is a consequence of the nontrivial renormalization of γ within a single layer, responsible for $\beta<1$ and $z>2$ for elastic depinning.

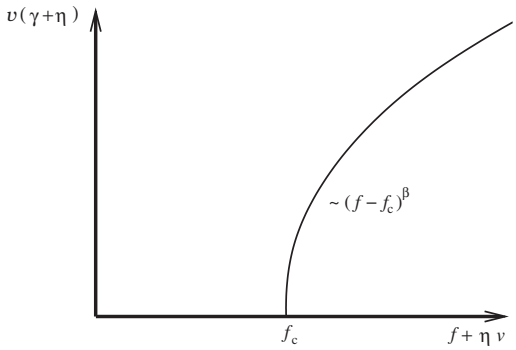

FIG. 4. The mean velocity $(\gamma+\eta)v$ plotted as a function of $F=f+\eta v$. When $f+\eta v$ is used as the independent variable, the velocity-force characteristic has the same functional form as that of a single elastic layer that depins at a threshold f_c with $v\sim(f-f_c)^\beta$ and $\beta<1$ as $f\to f_c^+$.

As pointed out in Ref. 80, the self-consistent single-layer approximation, with uniform couplings across the layers, is equivalent to a model of charge density waves (CDWs) that incorporates the coupling of the CDW to normal carriers via the addition of a global velocity coupling to the equation of motion for the phase.[73,101,102] Finally, another "partial" mean-field theory is obtained by assuming uniform couplings of strength $K_{\ell m}=K/N$ for every ℓ,m within each layer. This model will be discussed elsewhere. The two-particle toy model described in Sec. V corresponds to the $K=0$ limit of this mean-field theory.

III. FUNCTIONAL RG TO ONE LOOP

To go beyond mean field we now develop a functional RG approach.

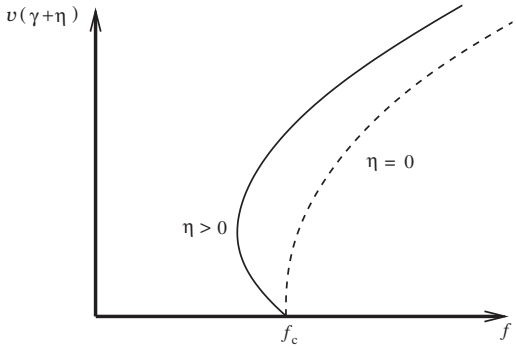

FIG. 5. The velocity-force curve for finite η can be obtained from the single-layer curve of Fig. 4 corresponding to $\eta=0$ (dashed line) by a change of the independent variable. Since $\beta<1$, the resulting $v(f)$ will be multivalued for any finite η.

A. Perturbation theory and length scales

Consider model (1.5) driven by a force f and assume that it reaches a time-translational invariant steady state (e.g., with periodic boundary conditions for each layer). There are two modes:

$$u^+ = (u^1 + u^2)/2, \quad u^- = u^1 - u^2. \tag{3.1}$$

For a system of finite size L, because of fluctuations in the pinning force, the velocity in each layer will be different. However this effect should disappear in the infinite-L limit, and can be suppressed using appropriate boundary conditions. Hence, we define v to be the velocity of the center of mass $v=\overline{\dot{u}^+}$, perform the shift to the comoving frame,

$$u^i = vt + \hat{u}^i, \tag{3.2}$$

and immediately drop the hat. We can now write the dynamical action associated to the resulting equation of motion [i.e., Eq. (1.5) shifted]:

$$\mathcal{S}[u,\tilde{u}] = \int_{x,t} \begin{pmatrix} \tilde{u}^1_{x,t} \\ \tilde{u}^2_{x,t} \end{pmatrix} \left[\begin{pmatrix} \gamma^0_{11} & \gamma^0_{12} \\ \gamma^0_{12} & \gamma^0_{11} \end{pmatrix} \frac{\mathrm{d}}{\mathrm{d}t} \begin{pmatrix} u^1_{x,t} \\ u^2_{x,t} \end{pmatrix} - c\nabla^2 \begin{pmatrix} u^1_{x,t} \\ u^2_{x,t} \end{pmatrix} \right] - \int_{x,t} (f - \gamma^0_+ v) \begin{pmatrix} \tilde{u}^1_{x,t} \\ \tilde{u}^2_{x,t} \end{pmatrix}$$
$$- \frac{1}{2} \int_{x,t,t'} \begin{pmatrix} \tilde{u}^1_{x,t} \\ \tilde{u}^2_{x,t} \end{pmatrix} \begin{pmatrix} \Delta_0(u^1_{x,t} - u^1_{x,t'} + v(t-t')) & 0 \\ 0 & \Delta_0(u^2_{x,t} - u^2_{x,t'} + v(t-t')) \end{pmatrix} \begin{pmatrix} \tilde{u}^1_{x,t} \\ \tilde{u}^2_{x,t} \end{pmatrix}. \tag{3.3}$$

The subscript 0 indicates that these are quantities for the bare model (and it is often dropped in the following). The matrix of friction coefficients is diagonal in basis (3.1) and we denote the frictions associated to the center of mass and relative motion as

$$\gamma_+ = \gamma_{11} + \gamma_{12}, \quad \gamma_- = \gamma_{11} - \gamma_{12}. \tag{3.4}$$

The bare values are $\gamma^0_+ = \gamma_0$ and $\gamma^0_- = \gamma_0 + 2\eta_0$. The bare response functions, i.e., those in the absence of disorder, read

$$R^{ij}_{k,t} := \langle u^i_{kt} \tilde{u}^j_{-k,0} \rangle_0, \tag{3.5}$$

$$R^{11}_{k,t} \equiv R^{22}_{k,t} = \Theta(t) \left[\frac{e^{-tk^2/\gamma_+}}{2\gamma_+} + \frac{e^{-tk^2/\gamma_-}}{2\gamma_-} \right], \tag{3.6}$$

$$R^{12}_{k,t} \equiv R^{21}_{k,t} = \Theta(t) \left[\frac{e^{-tk^2/\gamma_+}}{2\gamma_+} - \frac{e^{-tk^2/\gamma_-}}{2\gamma_-} \right]. \tag{3.7}$$

The case of a single layer is reproduced upon setting $\eta_0=0$, or equivalently $\gamma_-=\gamma_+$ (then $R^{11}_{kt} \to R_{kt}$, the standard single-layer response function, and $R^{12}_{k,t} \to 0$).

Writing $S=S_0+S_{\mathrm{int}}$ where S_{int} contains only the disorder, i.e., the second line in Eq. (3.3), the effective action $\Gamma[u]$ of the system can be computed perturbatively in the disorder:

$$\Gamma[u,\tilde{u}] = S_0[u,\tilde{u}] + \langle S_{\mathrm{int}}[u,\tilde{u}] \rangle_{S_0} + \frac{1}{2} \langle S_{\mathrm{int}}[u,\tilde{u}]^2 \rangle^c_{S_0} + \cdots \tag{3.8}$$

In the average over S_0 only one-particle irreducible (1PI) diagrams (i.e., containing loops) are kept. The quadratic part of the effective action yields the exact disorder-averaged response and correlation functions:

$$\mathcal{R}^{ij}_{q,t-t'} = \left. \frac{\delta^2 \Gamma[u,\tilde{u}]}{\delta \tilde{u}^i_{-qt'} \delta u^j_{qt}} \right|_{u=\tilde{u}=0},$$

$$\overline{u^i_{qt} u^j_{-qt'}} := \mathcal{C}^{ij}_{q,t-t'} = \mathcal{R}^{ik}_{q,t-t_1} \mathcal{R}^{jl}_{q,t-t_2} \left. \frac{\delta^2 \Gamma[u,\tilde{u}]}{\delta \tilde{u}^k_{-qt_1} \delta \tilde{u}^l_{qt_2}} \right|_{u=\tilde{u}=0}. \tag{3.9}$$

Both functions are symmetric in i,j and in q. The effective action has a complicated form but contains terms similar to those in the above action (3.3) with renormalized (i.e., "corrected") values for the friction matrix γ_{ij}, and the second cumulant of disorder $\Delta(u)$. The elastic term is unrenormalized (i.e., the zero-frequency part of the $\tilde{u}u$ term in Γ is the same as in S_0) thanks to the statistical tilt symmetry [the invariance of the nonlinear (i.e., disorder) terms of $\mathcal{S}$ under $u^i_{xt} \to u^i_{xt} + \phi^i(x)$ for two arbitrary static functions $\phi^i(x)$, $i=1,2$, should persist for Γ] which holds independently in each layer. Other terms are generated in perturbation theory, such as higher disorder cumulants, higher frequency corrections to the self-energy or nonlinear terms such as $\int \tilde{u}(\partial_t u)^2$. In each case their relevance should be assessed carefully. These terms are usually irrelevant near $d=4$. A simplifying feature is that the coupling between the layers is purely dynamical. Therefore the static part of the theory (i.e., the zero-frequency part of the effective action) consists of two decoupled static layers. This implies, among others, that no outer-diagonal elements of the disorder correlator are generated in perturbation theory.

Let us now examine perturbation theory and power counting. The effective action contains the term

$$-\tilde{f}\int_{xt}\sum_{i}\tilde{u}^{i}_{xt},\quad \tilde{f}=f-\gamma_0 v+\delta f(v), \tag{3.10}$$

where $\delta f(v)$ contains all corrections due to disorder. On average these are the same for each layer and depend on v. The equation of motion is obtained from the condition $\tilde{f}=0$ equivalent to $\langle u_{xt}\rangle=0$ (in shifted variables). From Eq. (3.8) one finds that to lowest order in Δ (i.e., to one loop) the corrections to friction and force are

$$\delta\gamma_{12}=0, \tag{3.11}$$

$$\delta\gamma_{11}=-\int_q\int_0^\infty \mathrm{d}\tau\tau\Delta''(v\tau)R^{11}_{q\tau}, \tag{3.12}$$

$$\delta f=\int_q\int_0^\infty \mathrm{d}\tau\Delta'(v\tau)R^{11}_{q\tau}, \tag{3.13}$$

where the index 0 is implicit if one studies perturbation theory on the bare action. The correction to the disorder Δ is of order Δ^2 and, at $v=0$, is identical to the one for a single-layer model, while at finite v it has a complicated expression (even in the single-layer case, as given in Ref. 16, not displayed here). As is well known, for $v=0^+$, $\Delta(u)$ acquires a cusp for scales larger than the Larkin length L_c.

Before obtaining the one-loop FRG equations let us make some general qualitative comments on the stability of the one-layer elastic quasistatic depinning to the viscous interlayer coupling. The absence of one-loop corrections to γ_{12} implies that to this order $\gamma_{12}=\gamma^0_{12}=-\eta_0$. Consider quasistatic depinning $v=0^+$. Then one finds

$$\delta\gamma_{11}=-\gamma_{11}\Delta''(0^+)\int_q\frac{1}{q^4}, \tag{3.14}$$

where a UV cutoff is implicit everywhere. This is the same correction as for the single-layer problem (i.e., for $v=0$ it does not depend on γ_{12}); hence under coarse graining γ_{11} is reduced compared to its bare value (above the Larkin scale L_c, $\Delta''(0^+)$ is strictly positive). The intralayer friction $\gamma_{11}<\gamma^0_{11}=\gamma_0+\eta_0$ remains finite and nonzero for $d>4$ (where the above integral converge at small q) while for $d\leq 4$ it becomes dependent on the system size L, $\gamma_{11}\approx(\gamma_0+\eta_0)(L/L_c)^{z-2}$, $z<2$ being the single-layer dynamical exponent for elastic depinning in $d<4$. Since γ_{12} is uncorrected (it is negative) and γ_{11} is reduced, it is clear that the friction coefficient of the center of mass of the system $\gamma_+=\gamma_{11}+\gamma_{12}$ may become negative at some scale, denoted by L_{pl}. When this occurs the fixed point of elastic quasistatic depinning becomes unstable (and inconsistent). This *always* occurs for $d<4$, but only for η_0 larger than a critical value η_c for $d>4$. The qualitative picture is then as follows:

(i) $d>4$: To lowest order the equation of motion reads

$$[\kappa(\gamma_0+\eta_0)-\eta_0]v=f-f_c+O(v_1^2), \tag{3.15}$$

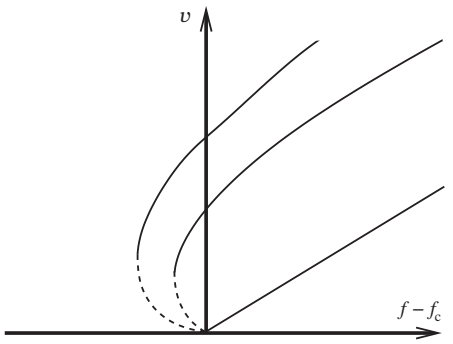

FIG. 6. Schematic $v-f$ curve corresponding to Eq. (3.19).

$$\kappa=\gamma_{11}/\gamma^0_{11}=1+\Delta''(0^+)\int_q\frac{1}{q^4}, \tag{3.16}$$

where we denote by $0<\kappa<1$ the usual reduction factor in friction in the single-layer problem. Elastic quasistatic depinning exists, with velocity

$$v\approx\frac{f-f_c}{\kappa(\gamma_0+\eta_0)-\eta_0}, \tag{3.17}$$

until the critical value of the interlayer coupling is reached,

$$\eta_0=\eta_c=\frac{\kappa}{1-\kappa}\gamma_0. \tag{3.18}$$

Here the reentrant (or hysteretic) branch appears. This is qualitatively similar to the mean-field picture. One can relate formally $(1-\kappa)\to M(c)\sim\overline{h^2}/c^2$ which for small disorder has the same form as Eq. (3.16), if the elastic coefficient (set to 1 in this section) is restored and one identifies $\Delta''(0)\to\overline{h^2}$. An interesting question is the nature of the elastic to hysteretic transition at η_c. Expanding Eq. (3.13) in powers of v yields the equation of motion near the critical point:

$$(\eta_c-\eta)v=f-f_c+2v^2(\gamma_{11}^2+\gamma_{12}^2)\Delta'''(0^+)\int_q\frac{1}{q^6}+O(v^3). \tag{3.19}$$

As one can see on Fig. 6, the transition is continuous if $\Delta'''(0^+)<0$ and $v\sim\sqrt{f-f_c}$ at the transition. (From the factor $\int_q q^{-6}$ one could identify $d=6$ as a critical dimension for the tricritical point and find that the terms $D\hat{u}\partial_t^2 u$ and $B\hat{u}(\partial_t u)^2$ both become relevant there. However one should remember that $\Delta'''(0)$ is irrelevant in $d=6$. Whether this modifies the exponents and leads to new universality class is left for future study.) Such a scenario may hold for the nonperiodic random manifold class. (For $d>4$, if the bare disorder is strong enough, $\Delta(u)$ develops a cusp; see Appendix in Ref. 103.) A series of higher multicritical points should exist, associated to correlators with leading behavior $\Delta^{(n+1)}(0^+)v^n$. For the periodic scalloped potential $n=\infty$ and the transition exhibit a jump or a quasijump (inverse logarithm) as in mean field, illustrated in Fig. 7.

(ii) $d<4$: the friction coefficient of the center of mass decreases with scale as

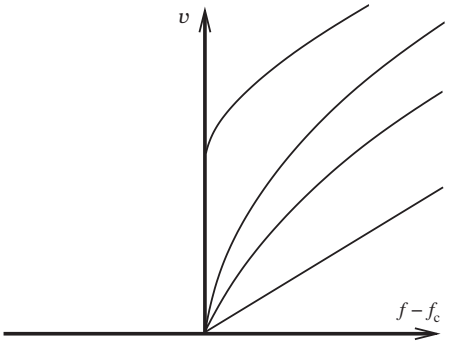

FIG. 7. Schematic $v-f$ curve corresponding to a sharp transition.

$$\gamma_+(L) \approx (\gamma_0 + \eta_0)(L_c/L)^{2-z} - \eta_0. \tag{3.20}$$

It reaches values near zero at a scale

$$L_{\rm pl} = L_c\left(\frac{\eta_0}{\gamma_0 + \eta_0}\right)^{-1/(2-z)}, \tag{3.21}$$

which diverges as $\eta_0 \to 0$, and which we term the "plastic length." Thus the depinning transition of a system of size $L < L_{\rm pl}$ remains similar to the standard (finite-size) elastic depinning of a single layer, while systems with $L > L_{\rm pl}$ cannot be described by single-layer elastic depinning. It is then likely that the system breaks into domains which can depin and move independently. We expect that our model applies for $L_{\rm pl} > L_{\rm disloc}$, where $L_{\rm disloc}$ is the length scale above which unbound dislocations appear in the system, generated for instance by a $\cos(u_1 - u_2)$ interlayer coupling. In our model interlayer dislocations occur at any finite velocity since they cost no energy and above $L_{\rm pl}$ the layers slip viscously. This regime could be interpreted as arising from a dense distribution of unbound dislocations along the interface between the two layers as shown in Ref. 104.

The full collective dynamics at scales $L > L_{\rm pl}$ however remains to be understood. This instability of the elastic depinning at finite scale is an effect beyond mean field.

Another important length scale is associated to a nonzero velocity. For single-layer elastic depinning it is

$$L_v \equiv L_v(\gamma_0) := L_c\left(\frac{\Lambda^2 r_f}{\gamma_0 v}\right)^{1/z}. \tag{3.22}$$

It is such that $v\tau = r_f$, where τ is the time scale diverging at depinning and r_f the correlation length of the disorder, equal to the period a (here set to unity) for the simplest CDW class. Beyond that scale the effect of quenched disorder is washed out into an effective thermal noise and the motion is uncorrelated. Equating the two scales $L_v(\gamma_0) = L_{\rm pl}$ defines a characteristic velocity scale,

$$\frac{\gamma_0 v_{\rm pl}}{\Lambda^2 r_f} = \left(\frac{\eta_0}{\gamma_0 + \eta_0}\right)^{z/(2-z)}, \tag{3.23}$$

below which plastic effects cannot be neglected. The behavior of the system at and beyond that scale still needs to be elucidated.

Since we found that the FRG fixed point of elastic depinning is dynamically *unstable* (to one loop) to the viscous coupling we now investigate the phase diagram of the moving phase.

B. Functional RG

Let us now derive and analyze the FRG equations to one-loop order at nonzero velocity. For pedagogical purposes, we use a Wilson scheme; i.e., we compute $\Gamma[u, \tilde{u}]$ to one loop using a cutoff $\Lambda_l = \Lambda e^{-l}$ and write RG equations as the cutoff is varied (i.e., integrating over a shell using $\int_{\Lambda_l e^{-dl} < q < \Lambda_l} f(q) = \tilde{S}_d \Lambda_l^d f(\Lambda_l) {\rm d}l$). A method which can handle higher loops, based on a nonzero mass scheme, is presented in Sec. IV. Here we restrict to the periodic problem and choose units such that the period is one.

The standard single-layer result for the correction to disorder upon integration over the shell can be expressed as

$$\partial_l \tilde{\Delta}(u) = \epsilon \tilde{\Delta}(u) - \frac{1}{2}[(\tilde{\Delta}(u) - \tilde{\Delta}(0))^2]'', \tag{3.24}$$

where one has defined $\tilde{\Delta}(u) = \tilde{S}_d \Lambda_l^{-\epsilon} \Delta(u)$. This result holds in the limit of zero velocity $v = 0^+$. As is well known, it results in a nonanalytic correlator beyond the Larkin length L_c. We note that a nonanalytic $\Delta(u)$ decreases γ, while an analytic correlator would increase it. We denote

$$\sigma = \Delta''(0^+), \quad \tilde{\sigma} = \tilde{\Delta}''(0^+). \tag{3.25}$$

The family of quadratic correlators,

$$\Delta(u) = \frac{\sigma}{2}\left[\frac{1}{6} - u(1-u)\right], \tag{3.26}$$

for $0 < u < 1$, periodically continued to all u, is preserved by the FRG flow, with $\partial_l \tilde{\sigma} = \epsilon\tilde{\sigma} - 3\tilde{\sigma}^2$. It is realized by a scalloped potential, or more generally by uncorrelated periodic shocks, and contains the universal fixed point of the random periodic (RP) class. For $\epsilon = 4 - d > 0$ it flows to $\tilde{\sigma}^* = 2 - z_{\rm el} = \epsilon/3$. For $d = 4$ the fixed point is at zero but the slow asymptotic decay $\tilde{\sigma} \sim 1/(3l)$ is universal.

Inserting formula (3.6) for the response function and the Fourier series $\Delta(u) = \Sigma_p e^{i2\pi p u} \Delta_p$ (over integer p) one finds the correction

$$\delta\gamma_{11} = \sigma \int_q \left[\frac{1}{2v^2\gamma_+}\Phi\left(\frac{q^2}{\gamma_+ v}\right) + \frac{1}{2v^2\gamma_-}\Phi\left(\frac{q^2}{\gamma_- v}\right)\right],$$

$$\Phi(x) := -\int_0^\infty du \frac{\Delta''(u)}{\Delta''(0^+)} u e^{-xu} = \sum_p \frac{(2\pi p)^2}{(x - i2\pi p)^2}\frac{\Delta_p}{\sigma}. \tag{3.27}$$

For the scalloped potential family (3.26) $\Delta_p = (1 - \delta_{p0})\sigma/(2\pi p)^2$, and $\Phi(x)$ reads

$$\Phi(x) = -\frac{1}{x^2} + \frac{1}{[2\sinh(x/2)]^2}. \tag{3.28}$$

In the sequel, we use the scalloped family (3.26) and form (3.28). From Eqs. (3.27) and (3.28) one obtains the RG equations

$$\partial_l \gamma_{11} = -\tilde{\sigma}\gamma_{11} + \frac{\tilde{\sigma}}{8v^2}\left[\frac{1}{\gamma_+}\frac{\Lambda_l^4}{\sinh^2\left(\frac{\Lambda_l^2}{2\gamma_+ v}\right)} + \frac{1}{\gamma_-}\frac{\Lambda_l^4}{\sinh^2\left(\frac{\Lambda_l^2}{2\gamma_- v}\right)}\right], \tag{3.29}$$

and of course $\partial_l \gamma_{12}=0$. For $v=0^+$ it reproduces the elastic depinning RG equation $\partial_l \gamma_{11} := (z_{\rm el}-2)\gamma_{11} = -\tilde{\sigma}\gamma_{11}$ which at the fixed point yields the dynamical exponent $z_{\rm el}=2-\epsilon/3$.

One can see from formula (3.29) that a nonzero velocity $v>0$ tends to cut the flow of γ_{11}. This is a usual effect in the case of elastic depinning ($\eta_0=0$) associated, in that case, to the single length scale $L_v(\gamma_0)$ defined in Eq. (3.22). Here there are *a priori* two length scales associated to the two modes u^+ and u^-. The effect of disorder is washed out only for scales larger than both lengths, i.e., if

$$\gamma_\pm v e^{2l}/\Lambda^2 \gg 1, \quad L > L_v^\pm. \tag{3.30}$$

Then the equation reduces to $\partial_l \gamma_{11} = -\frac{\tilde{\sigma}}{12}\frac{\Lambda^4}{\gamma_+\gamma_- v^2}e^{-4l}$. The difficulty is that $L_v^\pm$ are not simply equal to $L_v(\gamma_\pm^0)$ since the $\gamma_\pm(l)$ do not behave as the single-layer coupling (it does only for scales $L<L_{\rm pl}$). In fact, $\gamma_+(l)$ may vanish at some scale, hence the condition $\gamma_+(l)ve^{2l}/\Lambda^2 \gg 1$ may never be fulfilled, at *any* scale. A more careful analysis, performed below, is thus required.

One notes that Eq. (3.29) is the derivative $\partial_l \gamma_{11} = \partial_l \gamma_+ = -\partial_v \partial_l \tilde{f}$ with

$$\partial_l \tilde{f} = \gamma_{11}\tilde{\sigma}v - \frac{1}{4}\tilde{\sigma}\Lambda_l^2\left[\coth\left(\frac{\Lambda_l^2}{2\gamma_+ v}\right) + \coth\left(\frac{\Lambda_l^2}{2\gamma_- v}\right)\right] \tag{3.31}$$

from which the velocity-force characteristic is obtained as

$$f(v) = \gamma_0 v - \int_0^\infty {\rm d}l \partial_l \tilde{f}. \tag{3.32}$$

In the limit $v=0^+$ one recovers $\partial_l \tilde{f} = -\frac{1}{2}\tilde{\sigma}\Lambda_l^2$ which integrates to $-f_c^{\rm el,sl} = -\frac{1}{4}\tilde{\sigma}\Lambda^2$, the critical force of a single elastic layer. One notes the general relation,

$$\partial_v f(v) = \gamma_+, \tag{3.33}$$

valid for $l=\infty$, or for any intermediate scale, if one defines a finite-scale curve for $f(v)$ by setting the upper integration bound to l in Eq. (3.32).

We now study the flow of γ_{11} which depends on $\gamma_+ = \gamma_{11} - \eta_0$ and $\gamma_- = \gamma_+ + 2\eta_0$. We recall that the starting value is $\gamma_{11}^0 = \gamma_0 + \eta_0$. If the velocity is large enough, although γ_+ decreases upon renormalization, the corrections may be weak enough so that it remains positive, even for $d<4$. In the latter case, there should always be a critical velocity v_c such that $\gamma_+(l=\infty)=0$. For $v>v_c$ the $v(f)$ curve is well defined and continuous. For $v<v_c$ there is no moving solution such that $v(f)$ has a positive slope. Hence in a fixed-applied-force ensemble there is a jump to the pinned phase as the force is decreased. At $v=v_c^+$, from Eq. (3.33) the slope of the $v(f)$ curve is infinite. This corresponds to the minimal force $f_c^<$ at which the jump must occur. By contrast, when the force is increased in the pinned phase the critical force is $f_c^> = f_c^{\rm el,sl}$. It corresponds to the maximal force at which the jump upward in velocity to the moving state must occur. (In some cases it was observed that the jump can occur before these extremal values, either due to finite-size effects or due to a dynamical instability, which is beyond the present description.) At $v=v_c^+$ the length L_v^+ is *infinite*. This suggests that motion should be correlated on all scales, and that this point is very much like a critical point where scale invariance holds. An example of a $v(f)$ curve predicted by the one-loop FRG is given in Fig. 8.

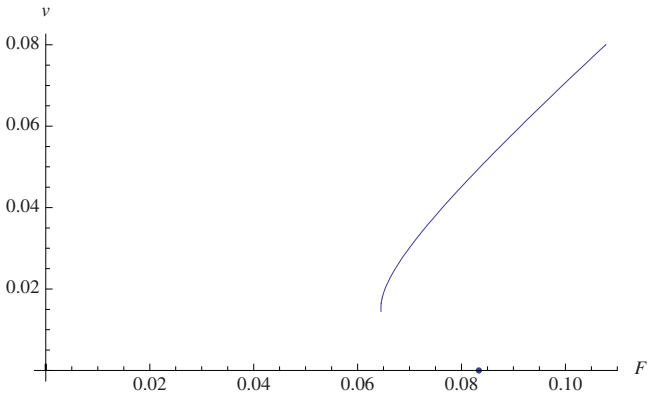

FIG. 8. (Color online) $v(F)$ curve obtained by integration of the one-loop equations in the text, for $\Lambda=1$, $\tilde{\sigma}=1/3$ ($\epsilon=1$) $\eta_0=10$, $\gamma_0=1$.

To estimate the jump velocity v_c it is simpler to first study a model where the bare value of γ_+, γ_0, is already small compared to γ_-, i.e., $\gamma_0 \ll \eta_0$. Then Eq. (3.29) can be approximated by

$$\partial_l \gamma_+ = -\tilde{\sigma}\eta_0 + \frac{\tilde{\sigma}\Lambda^4 e^{-4l}}{16\eta_0 v^2 \sinh^2\left(\frac{\Lambda^2 e^{-2l}}{4\eta_0 v}\right)}. \tag{3.34}$$

This is integrated into

$$\gamma_+(l=\infty) = \gamma_0 - \frac{1}{2}\tilde{\sigma}\eta_0 H\left(\frac{\Lambda^2}{4\eta_0 v}\right), \tag{3.35}$$

$$H(x) = \int_0^x \frac{{\rm d}y}{y}\left[1 - \frac{y^2}{\sinh^2(y)}\right] = -1 + x\coth(x) + \ln\left(\frac{x}{\sinh(x)}\right), \tag{3.36}$$

with $H(x) \approx \ln(2x) - 1$ at large x and $H(x) \approx \frac{x^2}{6}$ at small x. The critical velocity v_c is hence determined by

$$H\left(\frac{\Lambda^2}{4\eta_0 v_c}\right) = \frac{2}{\tilde{\sigma}}\frac{\gamma_0}{\eta_0}, \tag{3.37}$$

which gives the asymptotic behavior:

$$\frac{\eta_0 v_c}{\Lambda^2} \approx \frac{1}{2e}\exp\left(-\frac{2\gamma_0}{\tilde{\sigma}\eta_0}\right), \quad \frac{\tilde{\sigma}\eta_0}{\gamma_0} \ll 1, \tag{3.38}$$

$$\frac{\eta_0 v_c}{\Lambda^2} \approx \frac{1}{8}\left(\frac{\tilde{\sigma}\eta_0}{3\gamma_0}\right)^{1/2}, \quad \frac{\tilde{\sigma}\eta_0}{\gamma_0} \gg 1. \tag{3.39}$$

Here we have assumed $\tilde{\sigma}$ to be scale independent, hence a reasonable value for it is $\tilde{\sigma}=\sigma^*=2-z_{\rm el}=\epsilon/3+O(\epsilon^2)$. (Given the assumption $\gamma_0 \ll \eta_0$ the first regime exists only for small $\tilde{\sigma}$ which is either $\epsilon \to 0$ or if bare disorder is very small until the scale which controls the jump.) At the fixed point in $d=3,2,1$ the second regime is the relevant one and gives the value of the critical velocity for large η_0/γ_0.

To estimate the critical velocity when η_0/γ_0 is small, one must first integrate the flow up to scale l_1 at which $\gamma_+(l_1)=k\eta_0=k/(k+2)\gamma_-$ and k a number smaller than unity. Within this scale we can approximate $\gamma_{11}(l)=(\eta_0+\gamma_0)e^{-\tilde{\sigma}l}$, which yields $(\eta_0+\gamma_0)e^{-\tilde{\sigma}l_1}=(k+1)\eta_0$. The length scale $L_c e^{l_1}$ is on the order of the plastic length $L_{\rm pl}$ introduced above. Beyond that scale one can apply the previous analysis

$$\gamma_+(l=\infty)=\gamma_+(l_1)-\frac{1}{2}\tilde{\sigma}\eta_0 H\left(\frac{\Lambda^2}{4\eta_0 v e^{2l_1}}\right), \tag{3.40}$$

which yields the estimate

$$\frac{\eta_0 v_c}{\Lambda^2} \sim \left(\frac{(k+1)\eta_0}{\gamma_0+\eta_0}\right)^{2/\tilde{\sigma}} \frac{1}{4H^{-1}(2k/\tilde{\sigma})}. \tag{3.41}$$

Hence we find that the critical velocity vanishes as $\eta_0 v_c \sim (\eta_0/\gamma_0)^{2/(2-z)}$ in the limit of small viscous coupling, consistent with the estimate (3.23) for the scale at which plastic effects become important. The present one-loop analysis indicates however that the jump is always nonzero. (One notes that the flow of the disorder correlator, which is too complicated to analyze here, is also cut by velocity at the scale $\max(L_v^+, L_v^-)$. Hence, above that scale the parameter $\tilde{\sigma}$ cannot be assumed to take its fixed-point value and instead will decrease to zero. Since the effects computed here occur below these scales, one expects at most a change in the prefactors from taking these effects into account.)

It is instructive to compare with the predictions from mean-field theory (MFT) recalled in Sec. II A. In the regime of large viscous coupling $\eta_0 \gg \gamma_0$, one sees that formula (3.39) is very similar to the mean-field prediction

$$\eta_0 v_c = \frac{(c+h_0)}{2}\left(\frac{\eta_0}{3\gamma_0}\right)^{1/2}, \tag{3.42}$$

if one identifies $c+h_0 \to \sqrt{\tilde{\sigma}}/4$. Hence the one-loop FRG result, taken in the limit of large η_0, is very similar to MFT even for $d<4$, with the difference that the disorder parameter flows to a universal fixed value $\tilde{\sigma}^*$. In the other limit of small ratio η_0/γ_0, the result is very different from MFT because of the strong renormalization of the in-layer friction coefficient, and the threshold η_c which exists in mean field is zero for $d<4$.

It is also instructive to study the FRG flow for $d=4$ and $d>4$. For $d=4+\epsilon$ and a scalloped potential one has $\tilde{\sigma}=\tilde{\sigma}_0 e^{-\epsilon l}$, hence one finds at zero velocity $\gamma_{11}(l)=(\gamma_0+\eta_0)\exp[-\frac{\tilde{\sigma}_0}{\epsilon}(1-e^{-\epsilon l})]$ and $\gamma_+(l)=\gamma_{11}(l)-\eta_0$. There is thus a threshold for the jump in the $v(f)$ curve; it occurs only for $\eta_0 > \eta_c$ with

$$\eta_c = \frac{\gamma_0}{e^{\tilde{\sigma}_0/\epsilon}-1}. \tag{3.43}$$

η_c becomes very small as $d \to 4^+$. For $d=4$ one has $\tilde{\sigma}=1/(3l)$, hence $\gamma_{11}=(\gamma_0+\eta_0)/l^{1/3}$ and there is no threshold, $\eta_c=0$. The plastic length scale however diverges extremely fast as $L_{\rm pl}=L_c \exp[(\gamma_0/\eta_0)^3]$ for small η_0.

The analysis of this section relied on our preliminary finding that γ_{12} is not corrected. We now turn to a two-loop analysis to check whether this holds to higher orders.

IV. ANALYSIS INCLUDING TWO-LOOP CORRECTIONS

In this section we compute the corrections which arise at two loops around the quasistatic elastic depinning transition of the single layer at $f=f_c^{\rm el,sl}$. The calculation is performed in the limit $v \to 0^+$. The FRG flow is discussed separately for the nonperiodic and for the periodic cases. Possible consequences at nonzero v are discussed in each section.

The natural setting for higher-loop calculations is to use a mass as an infrared cutoff. It amounts to adding the force vector $m^2[w(t)-u^i_{x,t}]$ to the right-hand side of the equation of motion (1.5). It describes two layers both pulled by a spring attached to a point at position $w(t)$ which performs quasistatic forward motion. In that setting, it was shown[105] that the force correlator $\Delta(u)$ computed in the FRG is an observable related to the mean-square center-of-mass fluctuation around $w(t)$ in each layer. One introduces the rescaled correlator

$$\tilde{\Delta}(u) = C_d m^{-\epsilon+2\zeta}\Delta(u m^{-\zeta}), \tag{4.1}$$

where $C_d=\epsilon\tilde{I}_2=\epsilon\int_k (k^2+1)^2$ for $\epsilon=4-d>0$. One finds that $\tilde{\Delta}(u)$ converges to a fixed point, and to one-loop order it reproduces the Wilson approach.

A. Two-loop FRG equations

The two-loop FRG flow equation for the disorder is taken to be the same as the one derived in Ref. 18 at the quasistatic depinning transition:

$$\partial_\ell \Delta(u) = (\epsilon-2\zeta)\Delta(u) + \zeta u \Delta'(u) - \frac{1}{2}\{[\tilde{\Delta}(u)-\tilde{\Delta}(0)]^2\}'' + \frac{1}{2}\{[\tilde{\Delta}(u)-\tilde{\Delta}(0)]\tilde{\Delta}'(u)^2\}'' + \frac{1}{2}\tilde{\Delta}'(0^+)^2\tilde{\Delta}''(u), \tag{4.2}$$

where $\partial_\ell := -m\partial_m$. As explained there, the derivation of this FRG equation at two loops (especially the last term) relies on the Middleton theorem[23] which states that if all local velocities are positive at some time, they remain so at all times. In the two-layer viscous problem this property does not hold strictly, as backward motion of one layer is sometimes observed. The present calculation, thus, assumes that these effects can be neglected at large scale near the quasistatic depinning, and to this order.

The corrections to the friction coefficients are computed in Appendix B. They read

$$\partial_\ell \gamma_{12} = \frac{\gamma_{12}\tilde{\Delta}'(0^+)\tilde{\Delta}'''(0^+)}{2}\log\left|\frac{\gamma_{11}+\gamma_{12}}{\gamma_{11}-\gamma_{12}}\right|, \tag{4.3}$$

$$\partial_\ell \gamma_{11} = \gamma_{11}\left[-\tilde{\Delta}''(0)+\tilde{\Delta}''(0)^2+\tilde{\Delta}'''(0)\tilde{\Delta}'(0)\left(\frac{3}{2}-\ln 2\right)\right] + \frac{3\gamma_{12}\tilde{\Delta}'(0^+)\tilde{\Delta}'''(0^+)}{2}\log\left|\frac{\gamma_{11}+\gamma_{12}}{\gamma_{11}-\gamma_{12}}\right| + \gamma_{11}\tilde{\Delta}'(0^+)\tilde{\Delta}'''(0^+)\log\left|1-\frac{\gamma_{12}^2}{\gamma_{11}^2}\right|. \tag{4.4}$$

The calculation was performed in the physical domain $\gamma_+, \gamma_- > 0$. For mainly illustrative purpose, an analytical continuation was performed to the domain with negative friction coefficients, which yield the absolute values above. We find however that whenever the coefficients of the log terms are nonzero, the solution of the flow, obtained below, remains in the physical region.

It turns out that the two combinations $\tilde{\Delta}''(0^+)$ and $\tilde{\Delta}'(0^+)\tilde{\Delta}'''(0^+)$ which appear in these equations are universal numbers which can be related to the roughness exponent, ζ [using derivatives of Eq. (4.2) at $u=0$], independently of the precise form of the fixed point:

$$\tilde{\Delta}''(0) = \frac{1-\zeta_1}{3}\epsilon + \frac{\zeta_1^2-3\zeta_1-3\zeta_2+2}{9}\epsilon^2 + O(\epsilon^3),$$

$$\tilde{\Delta}'(0)\tilde{\Delta}^{(3)}(0) = \frac{(1-\zeta_1)\zeta_1}{12}\epsilon^2 + O(\epsilon^3). \tag{4.5}$$

Here we have defined

$$\zeta = \zeta_1\epsilon + \zeta_2\epsilon^2 + O(\epsilon^3). \tag{4.6}$$

B. Nonperiodic problem

As shown in Ref. 18 for a wide range of microscopic disorders, there is a unique elastic-depinning fixed point, calculated there, and identical at one loop to the random-field (RF) disorder class. At this fixed point one finds $\zeta_1 = 1/3$ and $\zeta_2 = 1/(27\sqrt{2}\gamma)$ with $\gamma = 0.5482228\ldots$ This yields

$$\partial_\ell \gamma_{11} = \left(-0.0432087\epsilon^2 - \frac{2\epsilon}{9}\right)\gamma_{11} + \frac{1}{54}\log\left(1-\frac{\gamma_{12}^2}{\gamma_{11}^2}\right)\gamma_{11}\epsilon^2 + \frac{1}{36}\log\left(\frac{\gamma_{11}+\gamma_{12}}{\gamma_{11}-\gamma_{12}}\right)\gamma_{12}\epsilon^2, \tag{4.7}$$

$$\partial_\ell \gamma_{12} = \frac{1}{108}\epsilon^2\log\left(\frac{\gamma_{11}+\gamma_{12}}{\gamma_{11}-\gamma_{12}}\right)\gamma_{12}. \tag{4.8}$$

We integrated the flow equations numerically. The result is given in Fig. 9 for $\epsilon=1$ and in Fig. 10 for $\epsilon=4$, to illustrate how the flow changes with ϵ. Looking carefully, one sees that starting in the physical region $\gamma_+ > 0$, the unphysical region $\gamma_+ < 0$ is avoided. One also sees that γ_+ approaches zero quickly, at least for small ϵ.

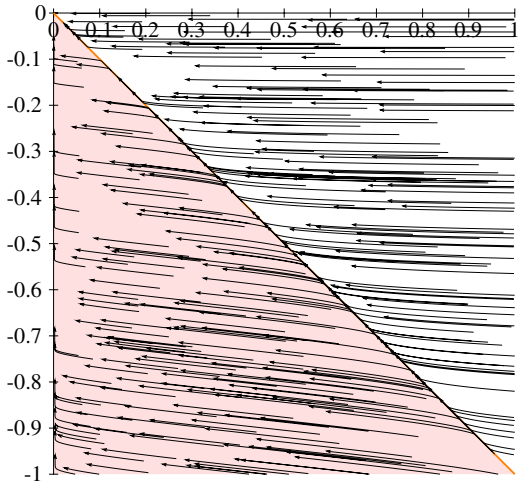

FIG. 9. (Color online) Flow of γ_{11} and γ_{12}, for $\epsilon=1$, as a function of γ_{11} (x axis) and γ_{12} (y axis). The separatrix is the diagonal line (orange) $\gamma_+ = \gamma_{11}+\gamma_{12}=0$. All physical initial conditions, corresponding to $\gamma_+ > 0$, remain physical. The shaded pink region corresponds to unphysical initial conditions $\gamma_+ < 0$.

We now confirm these two findings analytically. To do so, we change variables to $\gamma_+ = \gamma_{11}+\gamma_{12}$ and $\gamma_- = \gamma_{11}-\gamma_{12}$; see Eq. (1.6). We are interested in $\gamma_+ \approx 0$. There the flow equations become

$$\partial_\ell \gamma_+ = \epsilon\left(-0.009259\log\left(\frac{\gamma_+}{\gamma_-}\right)\epsilon - 0.008768\epsilon - \frac{1}{9}\right)\gamma_-,$$

$$\partial_\ell \gamma_- = -\left(\frac{1}{9}+0.008768\epsilon\right)\epsilon\gamma_-. \tag{4.9}$$

The second equation has the solution

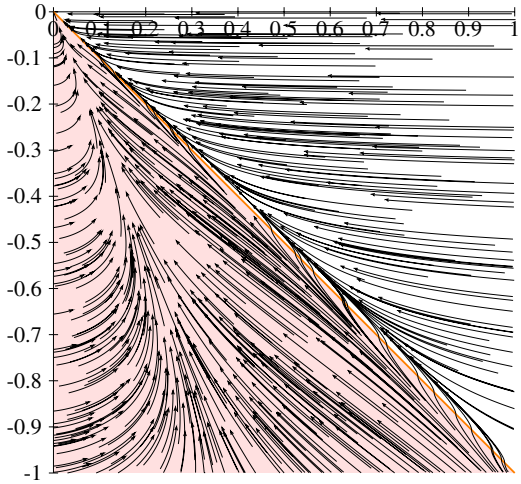

FIG. 10. (Color online) Flow of γ_{11} and γ_{12}, for $\epsilon=4$, as a function of γ_{11} (x axis) and γ_{12} (y axis). The separatrix (orange) is the line $\gamma_+ = \gamma_{11}+\gamma_{12}=0$. The pink region corresponds to unphysical initial conditions $\gamma_+ < 0$.

$$\gamma_-(\ell) = e^{-(1/9+0.008768\epsilon)\epsilon\ell}\gamma_-(0). \tag{4.10}$$

The solution for γ_+ is easily expressed as a function of γ_-, instead of ℓ:

$$\frac{d\gamma_+(\gamma_-)}{d\gamma_-} = 1 + \frac{\epsilon \log\left(\frac{\gamma_+(\gamma_-)}{\gamma_-}\right)}{12 + 0.94697\epsilon}. \tag{4.11}$$

The ratio

$$r(\gamma_-) := \frac{\gamma_+(\gamma_-)}{\gamma_-} \tag{4.12}$$

satisfies a closed flow equation as a function of γ_-:

$$-\frac{dr(\gamma_-)}{d\ln\gamma_-} = r(\gamma_-) - 1 - \frac{\epsilon \log r(\gamma_-)}{12 + 0.94697\epsilon}. \tag{4.13}$$

For all relevant values of ϵ $(0 \le \epsilon \le 4)$, there are two solutions: $r=1$ (unstable) and a nontrivial $(r^* \ll 1)$ solution of

$$r^* - 1 = \frac{\epsilon \log r^*}{12 + 0.94697\epsilon}, \tag{4.14}$$

which yields

$$r^* \approx \exp\left(-\frac{12 + 0.94697\epsilon}{\epsilon}\right). \tag{4.15}$$

The eigenvalue of the flow close to r^* is at leading order

$$y \approx -\frac{\epsilon^2 e^{12/\epsilon}}{108}. \tag{4.16}$$

Thus for ϵ small, this fixed point is very attractive. This is the fixed point obtained numerically above. It has the property that γ_+ remains strictly positive.

From Eq. (4.10) we extract the dynamical exponent associated with γ_-:

$$z_{\text{plastic}} = 2 - \frac{\epsilon}{9} - 0.008768\epsilon^2. \tag{4.17}$$

Since $\gamma_+ \approx r^* \gamma^-$, it has the same dynamical scaling, and the above z_{plastic} is indeed the critical exponent for the dynamics of both modes.

Hence within the two-loop analysis, and the stated assumptions, one finds a fixed point for the case of nonperiodic disorder. The dynamical exponent at this new fixed point deviates even at leading order in ϵ from the standard elastic depinning value:

$$z_{\text{elastic}} = 2 - \frac{2\epsilon}{9} - 0.0432087\epsilon^2. \tag{4.18}$$

Compared to one loop, the two-loop corrections appear singular, as seen from the $\ln(\gamma_-/\gamma_+)$ factors in the corrections to friction. As a result their magnitude is drastically enhanced above the plastic length L_{pl} from an expected $O(\epsilon^2)$ to an actual $O(\epsilon)$. The term $\tilde{\Delta}'(0^+)\tilde{\Delta}'''(0^+)\ln(\gamma_-/\gamma_+)$ in the correction to γ_{12} in Eq. (4.3) is in effect replaced, upon integration of the flow, by $\tilde{\Delta}''(0)$. This results in a value for $2-z$ twice smaller, to leading order, than the usual elastic fixed point.

To summarize, the one-loop analysis showed that γ_+ becomes very small near the plastic length, and provided a scenario for scales larger than L_{pl} which could sustain only a moving state at $v > v_c$. Although we did not perform the analysis for the nonperiodic case in detail we do not expect a difference at one loop. The present analysis—in the nonperiodic case—shows that additional physics occurs at two loops. It suggests that a $v=0^+$ state may still be possible. From the above analysis, one could surmise that it results in a very abrupt, almost vertical $v(f)$ curve (since γ_+ is found to converge very rapidly to a very small value) which is not strictly a jump, although it may look like one in a numerical calculation or an experiment. This "quasijump" would occur near the critical force of the elastic system, at variance with one loop. To confirm or infirm this scenario one would need to include the effects of a nonzero v, and a possible violation of the Middleton theorem within the two-loop theory, a challenge left for future work.

It also remains to be investigated to which extent the present analysis can be trusted in the region where γ_+ becomes very small, i.e., the region where $\ln(\gamma_-/\gamma_+)$ becomes of order $1/\epsilon$. We expect that in that region terms such as $\dot{u}^2$ in the equation of motion may become important. Such effects are presumably correctly resummed in the two-loop corrections and may explain why γ_+ remains positive. However since the counting of order in ϵ becomes unconventional if one follows the flow further in that region, there is no guarantee that higher loops may not lead to even more singular terms. In the best-case scenario only the $O(\epsilon^2)$ term in Eq. (4.18) would be changed by higher-loop corrections. Although the present results hint at a new depinning universality class with a dynamical exponent $z=z_{\text{pl}}$, a deeper understanding of the behavior of the system in the plastic region seems necessary before a firm conclusion can be drawn.

C. Periodic problem

The case of periodic disorder is also challenging. The quasistatic depinning fixed point has the form $\tilde{\Delta}(u) \sim u(1-u)$, as in Eq. (3.26) with

$$\tilde{\sigma} = \frac{\epsilon}{3} + \frac{\epsilon^2}{18} + \ldots, \tag{4.19}$$

and is expected to maintain that form to any order in ϵ. If the system is *exactly* at its fixed point, then, since $\tilde{\Delta}'''(0^+)=0$ at this fixed point, the flow equations for the γ's read

$$\partial_\ell \gamma_{12} = 0, \tag{4.20}$$

$$\partial_\ell \gamma_{11} = \gamma_{11}(-\tilde{\sigma} + \tilde{\sigma}^2) = -\gamma_{11}(2 - z_{\text{el}}), \tag{4.21}$$

$$z_{\text{el}} = 2 - \left(\frac{\epsilon}{3} + \frac{\epsilon^2}{9}\right). \tag{4.22}$$

Hence there are no drastic effects of the two-loop corrections, apart from changing the value of z: γ_{11} always decreases as in one-loop, γ_+ vanishes at some scale, and the one-loop analysis remains at least qualitatively correct. Hence this confirms the one-loop approach.

It is less obvious to understand the situation where the system is not exactly at its fixed point, but converges to it, i.e., $\tilde{\Delta}'''(0^+) \sim e^{-\epsilon l}$. Inserting this behavior in the above two-loop equations still results in drastic effects, i.e., γ_+ never crossing zero, again due to the logarithmic divergence of the corrections in that region, as for a nonperiodic problem. The discontinuous behavior between a zero and a small nonzero $\tilde{\Delta}'''(0^+)$ remains to be understood. One scenario which would save the agreement with the one-loop approach is that other irrelevant operators than $\Delta'''(0^+)$, neglected in the two-loop treatment of the periodic class, are equally important and modify the result back to Eq. (4.20). More work is clearly needed to settle these issues.

V. TOY MODELS WITH TWO PARTICLES

To gain insight on some of the issues arising in the dynamics of coupled elastic layers it is instructive to study the model in $d=0$, i.e., a toy model with two particles. This approach has proved useful for the elastic-depinning problem,[105] in particular in clarifying the information contained in the FRG functions. As we show below, a variety of behaviors arises already for two viscously coupled particles. Here we focus on the simplest situation of two particles in a periodic one-dimensional landscape driven by a force, and leave for future work the interesting nonperiodic case, as well as driving by a spring (which is more suitable for comparison with FRG). The model is thus the $d=0$ version of Eq. (2.1), with a pinning force $h^i Y(u^i - \beta^i)$; we choose $h^1 = h^2$ for simplicity. The random phase can be eliminated by a shift of the u^i, hence it is sufficient to study the case of two particles in the same landscape (up to a change in initial conditions). We first study smooth disorder, and then a scalloped landscape. (If an additional self-consistency condition is imposed, these models can also be used to implement a third mean-field approach discussed at the end of Sec. II A.)

A. Smooth potentials

We now study the following model:

$$\gamma \dot{u}_1 = \eta(\dot{u}_2 - \dot{u}_1) + f + \hat{\phi}(u_1), \tag{5.1}$$

$$\gamma \dot{u}_2 = \eta(\dot{u}_1 - \dot{u}_2) + f + \hat{\phi}(u_2). \tag{5.2}$$

In this section we adopt slightly different notations for center-of-mass and difference coordinates:

$$y = \frac{u_1 + u_2}{2}, \tag{5.3}$$

$$x = u_1 - u_2. \tag{5.4}$$

In these coordinates, the equation of motion becomes

$$\dot{y} = F - \frac{1}{2}[\phi(y + x/2) + \phi(y - x/2)], \tag{5.5}$$

$$\dot{x} = a[\phi(y - x/2) - \phi(y + x/2)], \tag{5.6}$$

where we have defined

$$a = \frac{\gamma}{\gamma + 2\eta}, \tag{5.7}$$

$$\phi = -\frac{\hat{\phi}}{\gamma}, \tag{5.8}$$

$$F = \frac{f}{\gamma}. \tag{5.9}$$

For definiteness we consider the family of periodic-force landscapes:

$$\phi(u) = \frac{p_1 \sin(2\pi u) + p_2 \sin(4\pi u)}{\sqrt{\frac{5}{8} - \frac{1}{128 p_2^2} + p_2^2 + \left(\frac{1}{4} + \frac{1}{128 p_2^2}\right)\sqrt{(1 + 32 p_2^2)}}}. \tag{5.10}$$

They are normalized such that if one takes $|p_1| = 1$ (the standard choice made in the following) the single-particle critical depinning force is $F_c^{\mathrm{sp}} = \pm 1$ (i.e., $\max[\phi(u)] = \max[-\phi(u)] = 1$) for any p_2. It turns out that the single-harmonic case is nongeneric and one needs to include at least one other harmonics, i.e., $p_2 \neq 0$.

We have integrated these equations numerically and plotted the resulting flow in Figs. 11–13 for various values of f and p_2. (We are grateful to Alan Middleton for clarifying remarks during the analysis of these flows.) The center-of-mass coordinate y is plotted along the vertical axis, the relative displacement x along the horizontal axis.

It is instructive to start with the case $\eta = 0$ ($a = 1$) of two uncoupled particles given in Fig. 11. The vertical trajectories along the y axis at $x = 0$ or $x = 1$ correspond to the two particles either in the same position or shifted by one period. As the force is decreased below threshold (right to left) a pair of fully attractive and fully repulsive fixed points appears on these axes. The total phase space for $F < F_c^{\mathrm{sp}} = 1$ is fragmented in pinned regions which flow to one of these "pinned-phase" fixed points, corresponding either to the two particles pinned in the same well or pinned in two wells shifted by one period, depending on the initial condition. Note also the other zero-force fixed point which has one attractive and one repulsive direction and corresponds to one particle in a stable equilibrium position at the bottom of one well and the other in an unstable equilibrium position at a hill top. This fixed point controls the separatrices of the flow. This structure, obvious in the absence of a coupling, will persist, with some modification, for nonzero η.

Interesting physics happens when the viscous coupling η is increased. The case $a = 0.2$ is shown in Fig. 12. Exactly along the axis $x = 0$ and $x = 1$ the equation of motion has not changed and the same attractive pinning fixed points are present for $F < F_c^{\mathrm{sp}} = 1$. However, unbounded motion is now possible for smaller forces $F_c < F < F_c^{\mathrm{sp}} = 1$, and takes place away from the axis. The force chosen in Fig. 12 is $F = 0.6$. On Fig. 12(a) the case $p_2 = 0$ is represented. One can easily see that it is fully integrable and that each trajectory in the central region is exactly periodic and crosses the $y = 0, 1$ axis at the same x. The region where this flow occurs is delimited

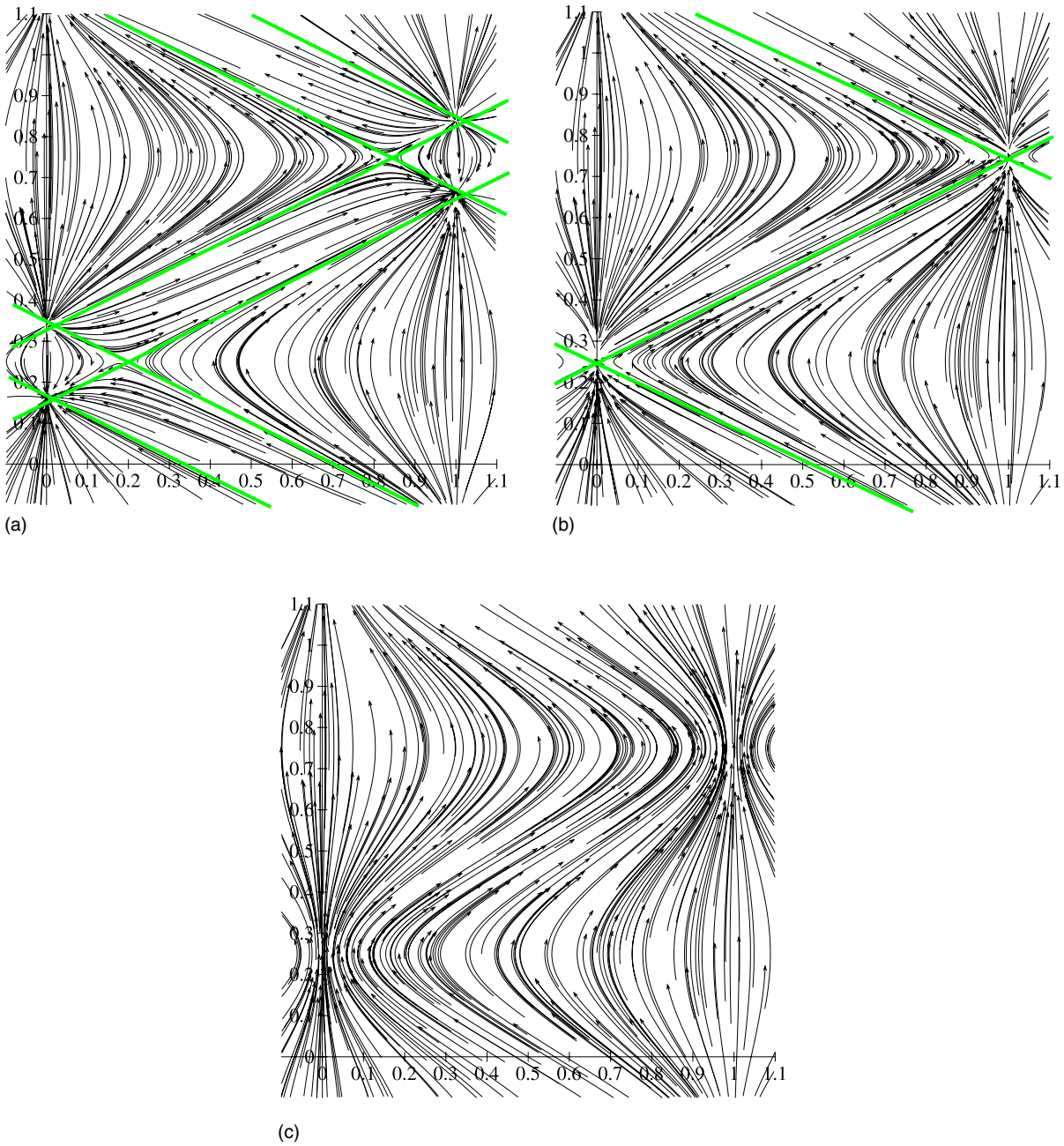

FIG. 11. (Color online) Uncoupled particles below depinning (a) ($F=0.85$), at depinning (b) ($F=1$) and above depinning (c) ($F=1.2$); $a=1$, $p_1=1$, $p_2=0$. We always plot x to the right and y to the top. Separatrices for the different attractive regions below threshold are drawn in green.

by the separatrices which meet at the above-mentioned zero-force saddle points. Hence, one sees clearly that the phase space splits into a pinned region and a flowing periodic region. In the case of a pure sine ($p_2=0$), this region is made of an infinity of neutral periodic trajectories (with zero Lyapunov exponent). In the more generic case $p_2 \neq 0$, the flowing region contains a single periodic trajectory. This trajectory is either attractive [case $p_2=0.5$, Fig. 12(b)] or repulsive [Fig. 12(c), with $p_2=-0.5$]. It is easy to prove from the symmetry properties of the flow that the Lyapunov exponent is reversed when the sign of the force landscape is reversed $\phi(u) \to -\phi(u)$. [Denoting $u^i(t,f,p_1,p_2)$ the solution of the equation of motion,for some given but unspecified initial condition, one sees that $u^i(t,-f,p_1,p_2)=-u^i(t,-f,p_1,p_2)$, $u^i(t,f,p_1,p_2)=1/2+u^i(t,f,-p_1,p_2)$, and $u^i(-t,f,-p_1,-p_2)=-u^i(-t,f,p_1,p_2)=1/2-u^i(-t,f,-p_1,p_2)$. This last property implies that Figs. 11(a) and 11(b) can be deduced by symmetry and that the Lyapunov exponent on the periodic trajectories (which are globally preserved by the symmetry) are reversed in sign. The pinned fixed points however remain attractive and are simply exchanged by this symmetry (they are not individually preserved).] In the repulsive case, any particle in the region *apparently flowing* on the figure eventually gets pinned at some larger y after visiting a few cells; the basin of attraction of the flowing phase has measure zero. This is an example where a nontrivial periodic stationary

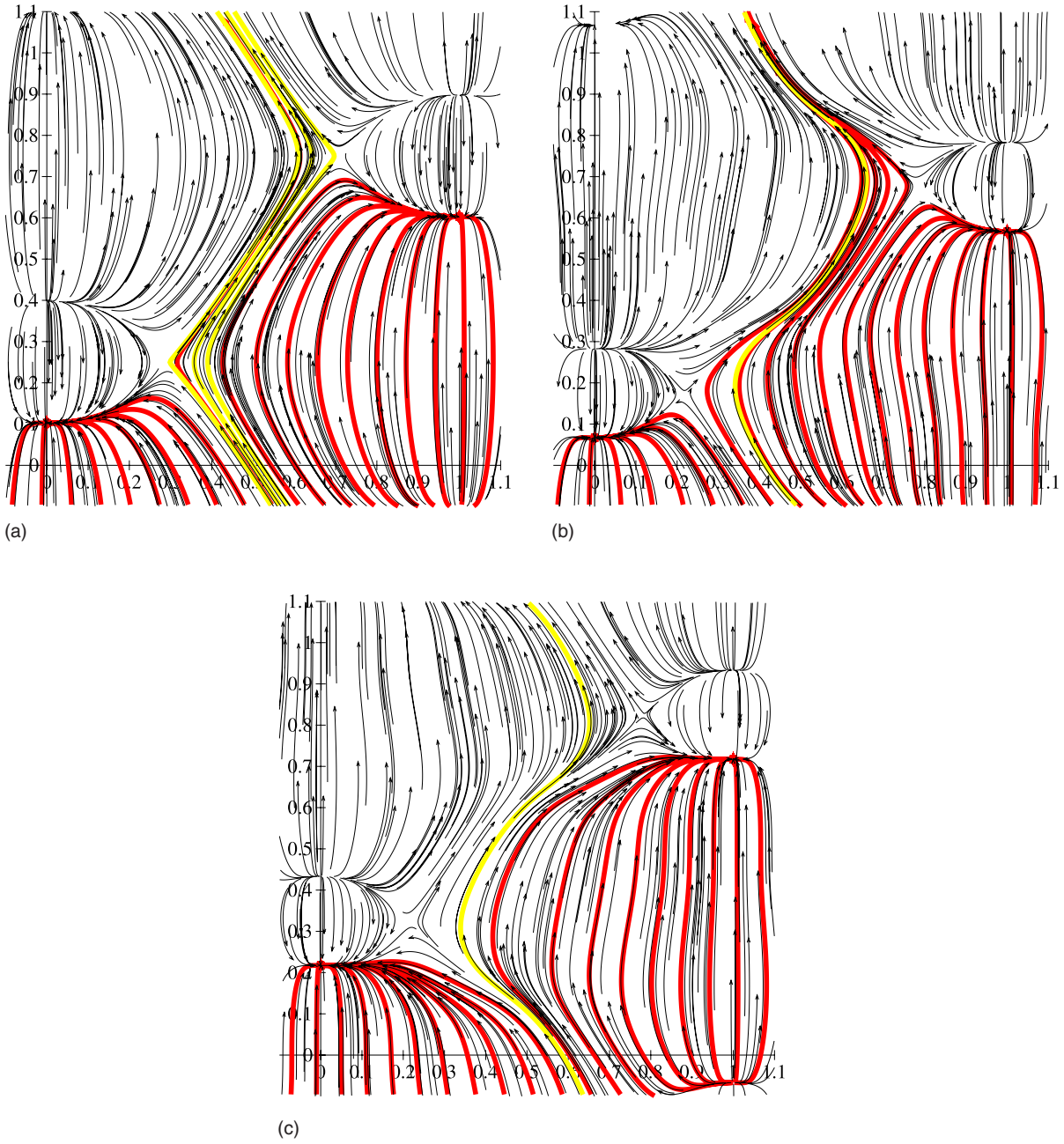

FIG. 12. (Color online) Viscously coupled particles ($a=0.2$) below depinning of the uncoupled particles ($F=0.6$). The anharmonic coefficient p_2 differs from left to right: $p_2=0$ (a); $p_2=0.5$ (b) and $p_2=-0.5$ (c). $p_1=1$. We plot 20 sample trajectories starting from $y=0$, and equally spaced in x. One sees that for $p_2>0$ more trajectories converge toward the unique stable solution (yellow). In the case of $p_2=0$, there is a family of periodic solutions, of which we have plotted three.

state exists, but is dynamically unstable. On the contrary, in the case $p_2=0.5$ [Fig. 12(b)] a distinct flowing phase exists, and its properties are dominated by a unique attractive periodic trajectory, and e.g., the average velocity is given by the inverse period of this trajectory. Finally Fig. 13 illustrates how the periodic orbit in the middle, hence the moving phase, disappears when the force is reduced below $F_c=0.522265$, leaving only a pinned phase for $F<F_c$.

We can now analyze the resulting $v(f)$ curve. The $v(f)$ curve for the pure-sine model is indicated schematically on Fig. 16(a) and is nongeneric, as discussed above. In the case $p_2\neq 0$ there are two branches corresponding to the two steady states, one (labeled 1) corresponding to the trajectory along the $x=0,1$ axis, i.e., the single particle $v(f)$ curve, and the second (labeled 2) corresponds to the periodic orbit near the middle of the figures, which generally has a higher $v(f)$ curve. If the second is repulsive ($p_2=-0.5$), then the trajectory along the $x=0,1$ axis is attractive: the global $v(f)$ curve then coincides with the single-particle one and there is no hysteresis of Fig. 16(b). If the second is attractive ($p_2=0.5$), the Lyapunov exponent of the periodic trajectories are inverted and the global $v(f)$ curve follows the second branch. (Note that while the line $x=0,1$ is always attractive in the vicinity of the pinned fixed points for $F<1$, it becomes—in

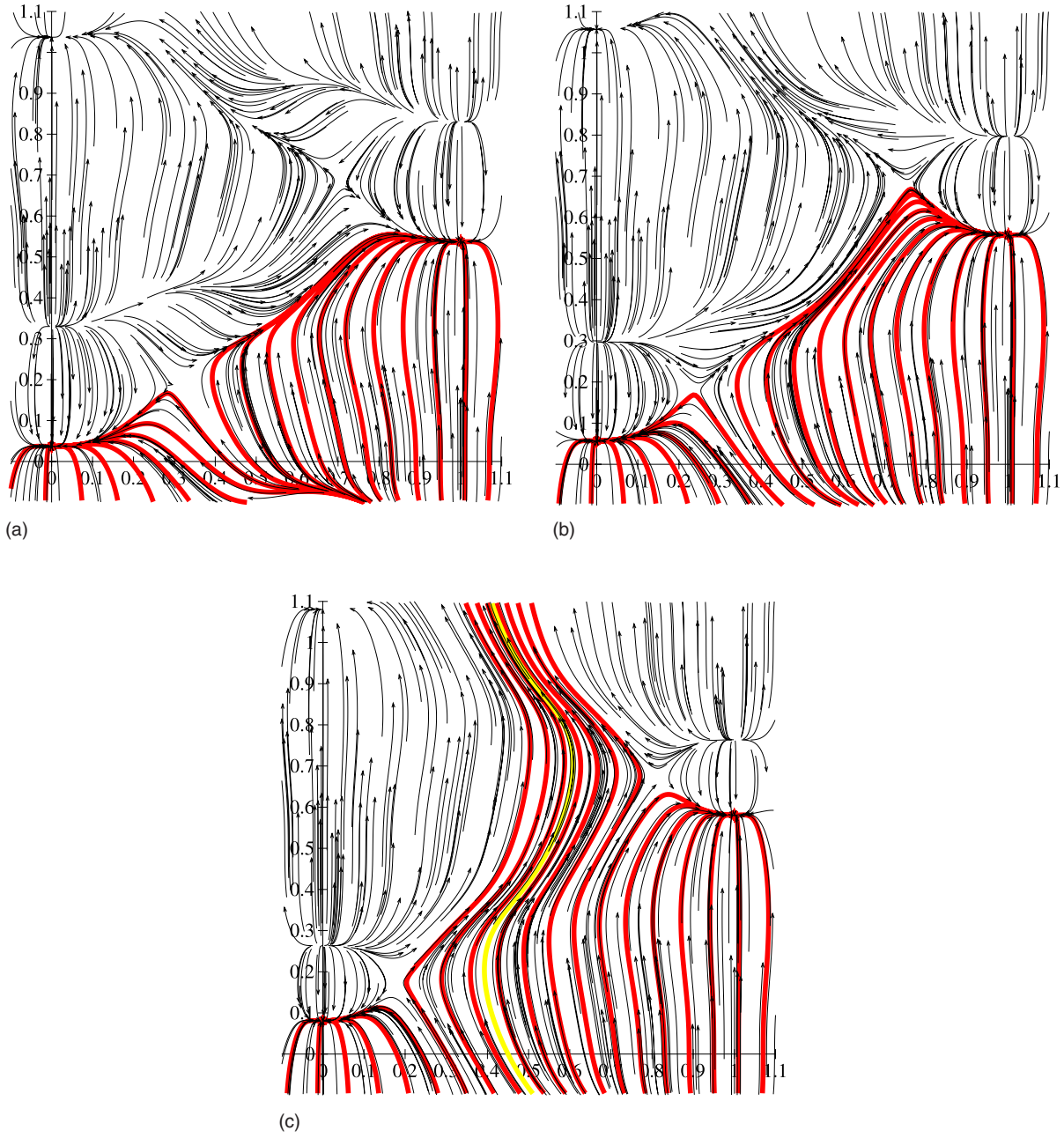

FIG. 13. (Color online) Viscously coupled particles ($a=0.2$) above (c) ($F=0.7$), at (b) ($F=F_c=0.522264$) and below depinning (a) ($F=0.35$). The anharmonic coefficient $p_2=0.5$. We plot 20 sample trajectories starting from $y=0$, and equally spaced in x. For (c) ($F=0.7$), we plot the unique stable solution (yellow). Even for this large F, one sees the convergence to this stable solution.

that case with $p_2=0.5$—repulsive for $F>1$ when the flow starts along this line. This is again a consequence of the symmetry properties mentioned above which inverts the Lyapunov along a periodic trajectory globally preserved by the symmetry.) In that case there is a hysteresis as the force is varied adiabatically; this is shown in Fig. 16(c). Upon decreasing the force from a large value the system follows the attractive trajectory in the middle until it disappears at F_c and the velocity vanishes. But if the force is increased from a value smaller than F_c, it can be seen from Fig. 13(a) that it first converges to a pinned fixed point along the axis $x=0,1$. Since these fixed points remain attractive up to $F=F_c^{\mathrm{sp}}=1$, the velocity remains zero until that force and then jumps to the stable moving state.

The question of whether a jump exists in the descending curve can be settled by analyzing how the periodic trajectory disappears at $F=F_c$. It can be seen from Fig. 13(b) that this occurs abruptly but that the period diverges at $F=F_c^+$ as the system spends more and more time near the zero-force saddle points. These hence play an important role in the transition at $F=F_c$. A simple argument indicates that the time spent near these points increases logarithmically, as is verified by the numerical integration of the flow in Figs. 14 and 15. Hence, although this system exhibits hysteresis in the

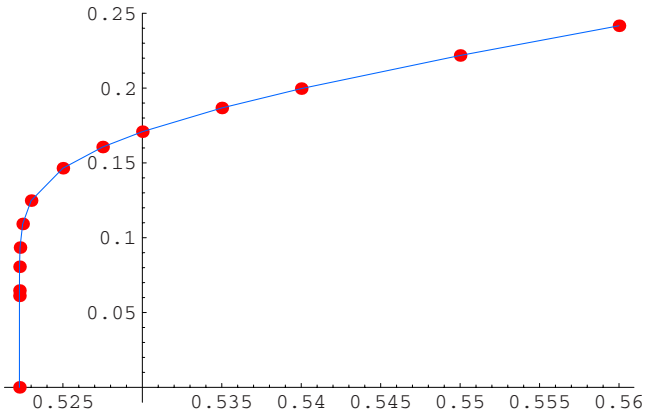

FIG. 14. (Color online) Velocity v as a function of F. The parameters used are $p_1=1$, $p_2=0.5$, $a=0.2$.

case $p_2=0.5$ it does not exhibit a velocity jump along the descending branch. Note that the critical behavior at F_c is different from the single-particle case $v\sim(F-F_c^{\mathrm{sp}})^{1/2}$ due to the zero-force saddle-point mechanism.

B. Scalloped potential

Here we consider the two-particle toy model for a piecewise parabolic (scalloped) potential, corresponding to a piecewise linear pinning force with jump discontinuities at the boundaries of each period. The equations of motion for the position of the particles are

$$\gamma\dot{u}_1=\eta(\dot{u}_2-\dot{u}_1)+f+\frac{1}{2}+n-u_1, \tag{5.11}$$

$$\gamma\dot{u}_2=\eta(\dot{u}_1-\dot{u}_2)+f+\frac{1}{2}+m-u_2 \tag{5.12}$$

for $n\le u_1\le n+1$ and $m\le u_2\le m+1$, with n and m integers.

When $\eta=0$, the particles are decoupled and the dynamics can be determined exactly. Each particle is pinned for $f<1/2$. For $f>1/2$ there is a unique periodic orbit of period

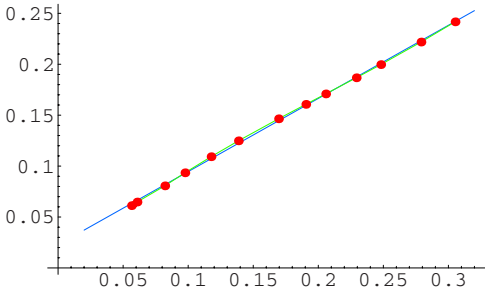

FIG. 15. (Color online) Velocity v as a function of $-1/\ln(F-F_c)$, with $F_c=0.522265$. The fit function is $v=0.0227714-0.718327/\ln(F-F_c)$. The linear fit is excellent. A (much worse) fit to a power law would give an exponent of about 0.1. The parameters used are $p_1=1$, $p_2=0.5$, and $a=0.2$.

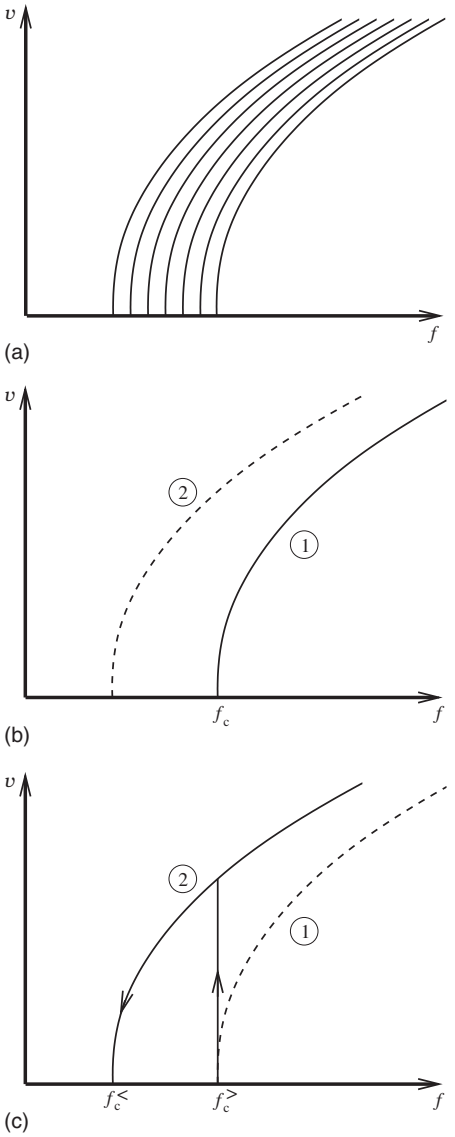

FIG. 16. Schematic $v(f)$ curves corresponding to the three cases discussed in the text: (a) single sine force landscape (b) the nontrivial periodic orbit 2 is repulsive and the $v(f)$ curve is the same as for a single particle 1 (c) the periodic orbit 2 is attractive and the $v(f)$ curve exhibits hysteresis as discussed in the text.

$$\frac{1}{v}=\gamma\ln\left(\frac{f+1/2}{f-1/2}\right) \tag{5.13}$$

that diverges linearly as $f\to(1/2)^+$. No periodic orbits exist for $f<1/2$ and the system does not exhibit hysteresis.

To consider the case $\eta\neq0$, we introduce center-of-mass and difference coordinates as in Eq. (5.3). In these new coordinates, the equations of motion are

$$\gamma\dot{y}=-y+f+\frac{1}{2}+\frac{n+m}{2}, \tag{5.14}$$

$$\gamma\dot{x}=-ax+a(n-m) \tag{5.15}$$

for $\frac{n+m}{2}\le y\le\frac{n+m}{2}+1$ and $n-(m+1)\le x\le 1+n-m$, with a given in Eq. (5.7).

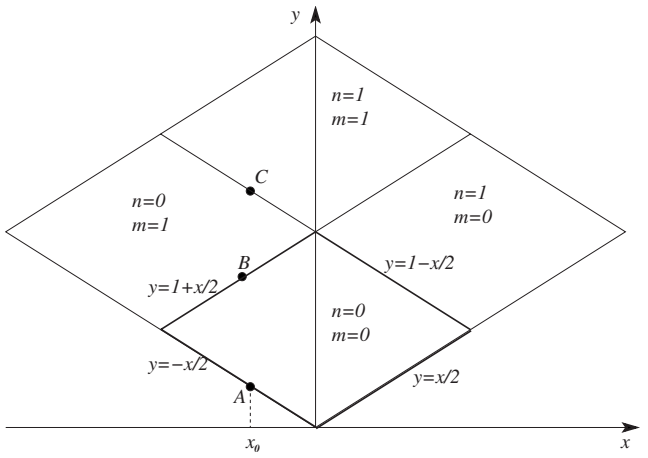

FIG. 17. The figure shows the boundaries of the regions where the relative and center-of-mass velocities of two particles in a periodic scalloped potential have jumps. The horizontal and vertical coordinates are the relative and center-of-mass position of the two particles, respectively, as defined in Eq. (5.3). The equations for the straight lines bounding the region corresponding to $n=0$, $m=0$ are indicated in bold.

Our goal is to identify the stable periodic orbits for this model and calculate the corresponding period or its inverse, the mean velocity. The regions in coordinate space corresponding to the various periods of the pinning potential are shown in Fig. 17. Consider a particle that starts at point A with $[x(0),y(0)]=(x_0,-x_0/2)$ in the region of the pinning potential corresponding to $(n,m)=(0,0)$. The boundaries of this region are defined by $-x/2\le y\le 1+x/2$, for $-1\le x\le 0$, and $x/2\le y\le 1-x/2$, for $0\le x\le 1$. This particle will travel across the (0,0) region to point B in a time $t_1(x_0)$ and then across the (0,1) region to a point C in a time $t_2(x_0)$, according to

$$A=\left(x_0,-\frac{x_0}{2}\right)\overset{t_1(x_0)}{\rightarrow}B=\left(x(t_1),1-\frac{|x(t_1)|}{2}\right)\overset{t_2(x_0)}{\rightarrow}C=\left(x(t_1+t_2),1+\frac{|x(t_1+t_2)|}{2}\right). \tag{5.16}$$

The case of a scalloped pinning potential can be studied analytically since the equations of motion are linear within each pinning period, with jump discontinuities in the velocity at boundaries of the pinning regions shown in Fig. 17.

1. Periodic orbits

We wish to determine the values of x_0 that correspond to periodic orbits as defined by the fixed point

$$x(t_1+t_2)\equiv x'(x_0)=x_0. \tag{5.17}$$

The period of such orbits is t_1+t_2 and $v=1/(t_1+t_2)$. It is convenient to introduce a new notation:

$$z_1(x_0)=e^{-t_1/\gamma}, \tag{5.18}$$

$$z_2(x_0)=e^{-t_2/\gamma}, \tag{5.19}$$

with

$$v=[\gamma\ln(1/z_1z_2)]^{-1}. \tag{5.20}$$

The dynamics from $(x_0,|x_0|/2)$ to $(x',1+|x'|/2)$ can be examined analytically since the equations of motion are piecewise linear. It is determined by

$$z_1\left(f+\frac{1}{2}-\frac{|x_0|}{2}\right)-\frac{|x_0|}{2}z_1^a=f-\frac{1}{2}, \tag{5.21}$$

$$fz_2-\frac{1}{2}z_2^a+\frac{|x_0|}{2}z_1^a(z_2+z_2^a)=f-\frac{1}{2}, \tag{5.22}$$

with

$$x'=x_0z_1^az_2^a+\frac{x_0}{|x_0|}(1-z_2^a). \tag{5.23}$$

We now look for a periodic solution or fixed point as defined by Eq. (5.1). Then Eq. (5.23) gives (provided $u_0\neq 0$)

$$|x_0|=\frac{1-z_2^a}{1-z_1^az_2^a}. \tag{5.24}$$

Substituting this in Eqs. (5.21) and (5.22) we obtain

$$z_1(f+1/2)-\frac{(1-z_2^a)(z_1+z_1^a)}{2(1-z_1^az_2^a)}=f-1/2, \tag{5.25}$$

$$z_2(f+1/2)-\frac{(1-z_1^a)(z_2+z_2^a)}{2(1-z_1^az_2^a)}=f-1/2. \tag{5.26}$$

These two equations are symmetric in z_1 and z_2, indicating that the solution must satisfy $z_1=z_2=z$. There is a fixed point x^* of x_0 where the system undergoes a periodic orbit of period $1/v=-2\ln(z)$, with

$$x^*=\frac{1}{1+z^a}, \tag{5.27}$$

$$z(f+1/2)-\frac{z+z^a}{2(1+z^a)}=f-1/2. \tag{5.28}$$

For any value of a we obtain $f(v)$ from Eq. (5.28), with the result

$$f=\frac{1}{2(1-z)}\left[1+z-\frac{z+z^a}{1+z^a}\right], \tag{5.29}$$

where

$$z=e^{-1/(2v)}. \tag{5.30}$$

The $v(f)$ curves obtained by inverting Eq. (5.29) are shown in Fig. 18 for a few values of a. These curves resemble those obtained in mean-field theory and suggest the possibility of a velocity jump. However, before making any conclusions we must study the stability of these periodic orbits. An analytic solution of Eq. (5.29) can be obtained for $a=1/2$.

For $a=1$, corresponding to $\eta=0$ (decoupled particles), x_0 is undetermined. For any x_0 one recovers the single-particle result given in Eq. (5.13). For instance, for $x_0=0$ we obtain

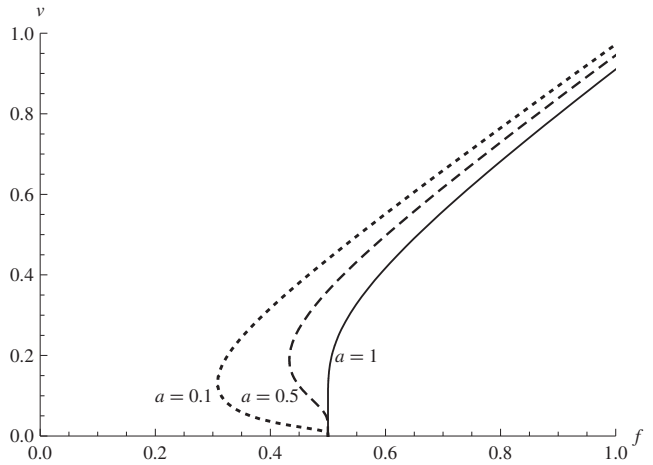

FIG. 18. The velocity-force characteristic obtained by inverting Eq. (5.29) for $a=1$ (solid line), corresponding to decoupled layers, $a=0.5$ (dashed line) and $a=0.1$ (dotted line).

$$z_1^* = \frac{f - 1/2}{f + 1/2}, \tag{5.31}$$

$$z_2^* = 1, \tag{5.32}$$

which yields Eq. (5.13).

2. Stability

The stability of the periodic solutions found in the preceding paragraph can be examined from the linear response to a perturbation of the initial condition. Letting $x_0 \to x_0^* + \delta x$, we define a Lyapunov exponent λ (by contrast to the Lyapunov exponent for a continuous-time flow defined in Sec. V A, this is the Lyapunov exponent for the discrete map, hence the transition of stable to unstable occurs as $|\lambda|$ crosses unity),

$$x'(x_0^* + \delta x) \equiv x_0^* + \lambda \delta x, \tag{5.33}$$

where $x'(x_0)$ is given by the right-hand side of Eq. (5.23). We find

$$\lambda = \left\{ \frac{z^{1+a}[a + z^a + 2f(1+z^a)]}{2fz(1+z^a) + z^{1+a} - az^a} \right\}^2. \tag{5.34}$$

At the fixed point z and f are related by Eq. (5.29). Inserting this into Eq. (5.34), we obtain

$$\lambda = \left\{ \frac{z^{1+a}[1 + z^a + a(1-z)]}{z(1+z^a) - az^a(1-z)} \right\}^2. \tag{5.35}$$

This Lyapunov exponent is plotted in Fig. 19 for a few values of a. It equals 1 for $a=0$ (corresponding to $\eta \to \infty$) and for $a=1$ (corresponding to $\eta=0$). For all other values of a one finds $\lambda < 1$ only for very small z, i.e., small v. This region corresponds to the part of the $v(f)$ curve that has negative slope near the depinning threshold $f=1/2$. The conclusion of this analysis is that this part is stable, while the portion with positive slope is unstable. This result is somewhat surprising in view of the results obtained in mean-field theory. However, as was explained in Sec. V A, reversing the sign of the force landscape would exchange the attractive and repulsive trajectories and result in the $v(f)$ curve more similar to the one shown in the mean-field section. The special nature of the two-particle scalloped-force landscape may be related to the absence of zero-force saddle points which played an important role in the case of the smooth potential. Note that we have not looked for more complicated periodic solutions, which are difficult to rule out.

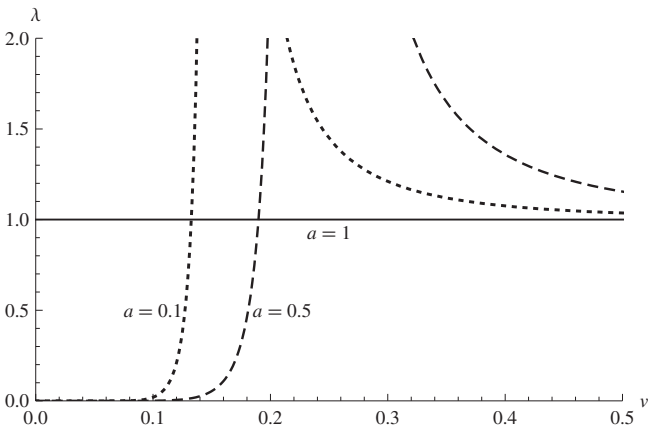

FIG. 19. The figure shows the Lyapunov exponent λ as function of v for $a=0.1$ (dotted), $a=0.5$ (dashed), and $a=1$ (solid). For $a=1$, $\lambda=1$.

C. Discussion of toy models

We conclude from Secs. V A and V B that a large variety of behaviors can already occur with two viscously coupled degrees of freedom in a random-force landscape. Understanding their systematics, for instance how one evolves from the smooth potential to the scalloped one as more harmonics are included, remains to be done. In each case one must identify the periodic trajectories and the attractor, whose structure may become more complex if the landscape contains more harmonics and more zero-force points. It is clear that an even more careful systematic study is necessary when increasing the number of degrees of freedom within these coupled layer models. It is not clear at this stage whether chaotic attractors exist, or whether even multiple stable periodic attractors do coexist.

VI. DISCUSSION

We have studied in this paper a model of two (single-component $N=1$) elastic layers driven over a random substrate and only coupled by a viscous coupling γ_{12}, going beyond mean-field theory. We have extended the functional RG approach which allows to describe the elastic depinning in each layer in the absence of an elastic coupling to the case of a nonzero γ_{12}. We have found that the FRG fixed point which describes elastic depinning is unstable to an arbitrarily weak viscous coupling beyond a plastic scale $L_{\rm pl}$ which diverges with a universal exponent as $\gamma_{12} \to 0$. To describe the plastic physics beyond that scale we have studied the FRG to one loop in the moving state at nonzero velocity. We found that the high-velocity branch of the $v(f)$ versus f curve terminates at a point $v=v_c$ where the slope is infinite. This point

corresponds to a force smaller than the elastic depinning threshold, hence there is a range of values of f where a pinned state coexists with a moving state. This dynamical hysteresis is very similar to the one found in mean-field theory. One could then conclude that the one-loop FRG result nicely confirms the main features of the mean-field theory and, in addition, allows to establish precise universal results and identify the proper length scales.

This conclusion may, however, be too hurried as, surprisingly, our two-loop calculation shows some possible problems with this picture. The calculation is based on certain assumptions (discussed in Sec. IV, i.e., the neglect of violations of Middleton's theorem, the neglect of higher orders in the region of small η_+) and more work is clearly needed to ascertain its validity. However, as a preliminary step it indicates a new universality class in the case of nonperiodic objects and in the periodic case, a possible breakdown of the one-loop picture depending on how irrelevant operators are taken into account. This possible alternative picture is the absence of a dynamical hysteresis and a nearly vertical $v(f)$ curve near the elastic threshold.

In an attempt to understand which effects could be missed by the mean-field and one-loop approaches, we have solved simple toy models in $d=0$. We found indeed that dynamical hysteresis may or may not be present depending on the realization of disorder. Although in all cases considered one finds a periodic trajectory with nonzero velocity which survives below the elastic (uncoupled) threshold, this trajectory may be attractive or repulsive depending on the disorder realization. It remains to be studied in detail how these properties carry to a larger number of degrees of freedom. In any case it cannot be assumed that a single attractive periodic attractor exists and a detailed study of such attractors as the number of particles increases must be done with care before any conclusion can be drawn.

The particle models also show the importance of the zero-force points in phase space. These are couples of configurations in the two layers (u_x^1, u_x^2) where all forces vanish. They are defined in the statics, hence are independent of the viscous coupling. However it is important to know their dynamical stability in presence of a viscous coupling. It is proved in Appendix A that metastable states, i.e., stable states where the energy has a local minimum, remain stable, i.e., dynamically attractive, at nonzero viscous coupling. This means that each pinned state, i.e., blocking configuration for each uncoupled layer, keeps a nonzero basin of attraction when the viscous coupling is increased from zero. In the absence of a viscous coupling, when upon increasing f such a pinned state becomes unstable, the next configuration is determined by the no-passing rule and Middleton's theorem, as the minimum over u of all metastable configurations in the direction of the force. In the presence of a viscous coupling, however, there is no guarantee that the system will not flow from there to a periodic orbit, resulting in a jump in the $v(f)$ curve. Thus even if the metastable zero-force couples remain attractive, they may not be easily *dynamically accessible*; i.e., their basin of attraction may shrink and be nearly invisible in a procedure such as force ramping. These effects, as well as the competition between the zero-force fixed points and the periodic orbits, clearly remain to be studied systematically.

It is thus a remaining challenge to understand how the FRG can describe the structure of such a complicated phase space with periodic orbits coexisting with pinned fixed points. It is probable that the FRG calculation presented here retains only averaged effects and does not address these issues with sufficient accuracy. One possible geometry to study this in a controlled manner starting with a particle and then extending to manifolds is to use the drive by a harmonic well. Since the coupling between the layers exists only when the system is moving, one needs to go beyond the present calculation and study, for instance, how the avalanches in the two layers are correlated.

In a broader context, one needs to justify why effort should be devoted to clarify the behavior of this simple two-layer model with viscous coupling only. This model indeed neglects the competition between plastic interlayer and elastic intralayer couplings, and one should question its range of validity. Since any small realistic interaction between two identical elastic layers, such as a crystal or a CDW in the absence of in-layer topological defects (which we have not included here), generates some small interlayer commensurate coupling, one should ask whether our model is stable to that. This can be analyzed by adding a force $-g_1 \sin[2\pi p(u_{xt}^1 - u_{xt}^2)]$, with $p=1$, to the equation of motion (1.5) of layer 1, and its opposite for layer 2. Such a coupling generates an elastic coupling at small scale between the layers, and if it is relevant in the RG sense, at large scales as well. In the latter situation the elastic coupling should dominate the viscous one and one expects that the system is described by elastic depinning. It was found in mean-field models that such a coupling is always relevant in the moving phase.[79] If such a result were general, the model studied here would be somewhat artificial, or describe only a limited range of length scales.

It is easy to compute, to one-loop accuracy and for any p, the linear eigenvalue of an infinitesimal perturbation $g_1 > 0$ at the unperturbed quasistatic depinning fixed point at $v = 0^+$ studied here. A first (and naive) calculation in the spirit of the statics yields

$$\partial_l \tilde{g}_1 = [2 - 4\pi^2 p^2 \tilde{\Delta}(0)]\tilde{g}_1, \tag{6.1}$$

where $\tilde{g}_1$ is the dimensionless coupling. This is essentially the result obtained for the problem of a single layer in presence of both disorder and a commensurate potential[106] up to a factor of 2 which accounts for the fact that the disorder exists in both layers, compared to Ref. 106. Inserting the value of $\tilde{\Delta}(0) = \epsilon/36$ at the one-loop depinning fixed point implies that this coupling is always relevant near $d=4$, which would seem to confirm the mean-field conclusion. It also yields a critical dimension near $d=2$, i.e., $4 - d_c \approx -18/\pi^2$ below which the coupling should become irrelevant. This conclusion is correct for the statics, but incorrect near the depinning threshold.

At depinning at least two new effects should be taken into account. First, one sees that the coupling g_1 generates in

perturbation theory a correction to the critical force, which amounts to adding *the same* force $-g_2\cos(2\pi p(u^1_{xt}-u^2_{xt}))$, with $p=1$, to the equation of motion (1.5) of each layer. These two terms feed into each other and the correct linearized RG equation takes the form, to one loop:

$$\begin{pmatrix} \partial_l \tilde{g}_1 \\ \partial_l \tilde{g}_2 \end{pmatrix} = \begin{pmatrix} 2-4\pi^2 p^2 \tilde{\Delta}(0) & -2\pi p \tilde{\Delta}'(0^+) \\ 2\pi p \tilde{\Delta}'(0^+) & 2-4\pi^2 p^2 \tilde{\Delta}(0) \end{pmatrix} \begin{pmatrix} \tilde{g}_1 \\ \tilde{g}_2 \end{pmatrix}. \tag{6.2}$$

Second, and most importantly, from the two-loop solution of the standard depinning fixed point,[18] we know that $\tilde{\Delta}(0)$ does not flow to a fixed point; it always increases as $\tilde{\Delta}(0)\sim e^{\epsilon l}\sim L^{\epsilon}$. Physically, a *static random force* is generated by the quenched disorder in the limit $v=0^+$. This is due to terms in the two-loop beta-function which account for the irreversibility of depinning and is at variance with the statics.[107] At depinning however, a small coupling between layers is always irrelevant for $d<4$. This can be seen from Eq. (6.2), since $\tilde{\Delta}(0)$ grows while $\tilde{\Delta}'(0^+)$ converges to a $O(\epsilon)$ fixed point. It justifies *a posteriori* the model studied in this paper. Of course at larger bare couplings it is likely that a coupled phase will arise and it would be interesting to study that transition.[108]

Let us finish by recalling that one issue in the theory of plastic flow is whether one can use $P(v)$, the distribution of time-averaged individual particle velocities, as a meaningful order parameter in the thermodynamics limit. One could then distinguish two classes of plastic flow: (i) flows with nontrivial $P(v)$ (e.g., pinned particles coexisting with flowing rivers) and (ii) flows with peaked $P(v)$ (a delta function in the large-size limit) but which cannot be described by a fully elastic theory. The layered model studied here is a tractable example of class (ii) and requires, to exhibit a nonzero depinning threshold, elastic interactions inside the layers. Models for class (i) have been studied, where particles interact only through a hard core interaction.[81] It would be quite interesting to find a tractable model which encompasses both classes and their possible transitions.

Finally, we have limited ourselves to the analysis of the mean velocity in the steady state. It would be interesting to examine the temporal noise and its power spectrum in the steady state, as well as avalanche distributions within each layer and their intralayer correlations. This is left for future work.

ACKNOWLEDGMENTS

We would like to thank Jennifer Schwarz for very useful interactions at the beginning of this work. We also acknowledge helpful discussions with Alan Middleton and Denis Bernard. M.C.M. was supported by the National Science Foundation through Grants No. DMR-0305407 DMR-0705105 and DMR-0806511 and through the Rotschild-Yvette-Mayent Foundation at the Institut Curie in Paris. She thanks the Institut Curie and ESPCI for their hospitality during the completion of some of this work. P.L.D. and K.W. acknowledge support from ANR under Program No. 05-BLAN-0099-01.

APPENDIX A: STABILITY OF ZERO-FORCE FIXED POINTS

Let us call u^i_x a static configuration where the force is zero, i.e., $F^i(u^i(x),x)=0$, $i=1,2$. The equation of motion linearized around the fixed point (FP) is

$$\begin{pmatrix} \dot{u}^1_{x,t} \\ \dot{u}^2_{x,t} \end{pmatrix} = M \begin{pmatrix} u^1_{x,t} \\ u^2_{x,t} \end{pmatrix}, \tag{A1}$$

$$M = AB = -\frac{1}{\gamma_{11}^2-\gamma_{12}^2}\begin{pmatrix} \gamma_{11}H_1 & -\gamma_{12}H_2 \\ -\gamma_{12}H_1 & \gamma_{11}H_2 \end{pmatrix}, \tag{A2}$$

$$A^{-1} = \begin{pmatrix} \gamma_{11} & \gamma_{12} \\ \gamma_{12} & \gamma_{11} \end{pmatrix}, \quad B = \begin{pmatrix} -H_1 & 0 \\ 0 & -H_2 \end{pmatrix}, \tag{A3}$$

and we are interested in the Lyapunov exponents or relaxation rates around the zero-force fixed point, i.e., the eigenvalues of the matrix M. We have introduced the Hessian $(H_i)_{xx'}=-\nabla_x^2\delta_{xx'}+V_i''(u^i_x,x)\delta_{xx'}$ in each layer, which are Hermitian matrices. They have eigenvalues μ_{i,α_i} and eigenvectors $\phi_{i,\alpha_i}(x)$. In the absence of a coupling between the layers ($\gamma_{12}=0$) the eigenvalues μ_{i,α_i} are proportional to the Lyapunov exponents, i.e., $\lambda_{i,\alpha_i}=-\gamma_{11}^{-1}\mu_{i,\alpha_i}$. A question is how they vary as the viscous coupling is increased. Note that one can decompose

$$u^i_{xt} = \sum_{\alpha_i} \phi_{i,\alpha_i}(x) u_{\alpha_i}(t), \tag{A4}$$

and in that basis the equation of motion reads

$$\sum_{\alpha_1',\alpha_2'} \begin{pmatrix} \gamma_{11}\delta_{\alpha_1,\alpha_1'} & \gamma_{12}\int_x \phi^*_{1,\alpha_1}(x)\phi_{2,\alpha_2'}(x) \\ \gamma_{12}\int_x \phi^*_{2,\alpha_2}(x)\phi_{1,\alpha_1'}(x) & \gamma_{11}\delta_{\alpha_2,\alpha_2'} \end{pmatrix} \begin{pmatrix} \dot{u}_{\alpha_1'}(t) \\ \dot{u}_{\alpha_2'}(t) \end{pmatrix} = -\begin{pmatrix} \mu_{1,\alpha_1}u_{\alpha_1}(t) \\ \mu_{2,\alpha_2}u_{\alpha_2}(t) \end{pmatrix}, \tag{A5}$$

since the velocity coupling between layers is local in space, it becomes nonlocal in the eigenstates of the two Hessians.

The matrix M has several interesting properties. Although it is not Hermitian, since A and B do not commute, its eigenvalues are real. Indeed, consider an eigenstate v such that $M \cdot v = \lambda v$. This implies $B \cdot v = \lambda A^{-1} \cdot v$, hence,

$$v^\dagger \cdot B \cdot v = \lambda v^\dagger \cdot A^{-1} \cdot v. \tag{A6}$$

Since B and A are Hermitian (and also real symmetric) matrices, $v^\dagger \cdot B \cdot v$ and $v^\dagger \cdot A^{-1} \cdot v$ are real, and thus λ is real.

Consider now a bare model such that A^{-1} is strictly positive definite with eigenvalues $\gamma_+ > 0$, $\gamma_- > 0$, i.e., $\gamma_{12}^2 < \gamma_{11}^2$. Then Eq. (A6) implies that the sign of λ is the same as the sign of $v^\dagger \cdot B \cdot v$. Let us consider a stable (i.e., attractive) zero-force point with all $\mu_{i,\alpha_i} > 0$, hence B is strictly negative definite. In its neighborhood in phase space, in the absence of viscous coupling between layers, the system is pinned. Since $v^\dagger \cdot B \cdot v < 0$ for any nonzero v, the above property implies that the zero-force fixed point remains stable; i.e., all Lyapunov exponents remain strictly negative, as the viscous coupling between layers $\gamma_{12}^2 < \gamma_{11}^2$ is increased, and Eq. (A6) implies the bounds

$$\frac{\mu_{\min}}{\gamma_-} < -\lambda < \frac{\mu_{\max}}{\gamma_+} \tag{A7}$$

for a model with $\gamma_{12} < 0$, and where $\mu_{\min}$ and $\mu_{\max}$ are the smallest and largest eigenvalues of $-B$.

These eigenvalues of stability can be obtained exactly in the case where H_1 and H_2 commute. Then one can choose the same basis in both layers $\phi_{1,\alpha}(x) = \phi_{2,\alpha}(x)$. The Lyapunov exponents, i.e., the eigenvalues λ in $\dot{u} = \lambda u$ of Eq. (A3) can then be organized in pairs with

$$\lambda_\alpha = -\frac{\gamma_{11}(\mu_{1,\alpha} + \mu_{2,\alpha})}{2(\gamma_{11}^2 - \gamma_{12}^2)} \pm \frac{\sqrt{\gamma_{11}^2(\mu_{1,\alpha} - \mu_{2,\alpha})^2 + 4\gamma_{12}^2 \mu_{1,\alpha}\mu_{2,\alpha}}}{2(\gamma_{11}^2 - \gamma_{12}^2)} \tag{A8}$$

and one checks that as long as $\gamma_+ = \gamma_{11} - \gamma_{12} > 0$ a stable FP remains stable as γ_{12}^2 is increased (this holds for the two-particle model considered above). In general one does not expect H_1 and H_2 to commute, since the disorders in the two layers are uncorrelated. For small interlayer coupling one can apply second-order perturbation theory,

$$\lambda_{1,\alpha_1} = -\frac{\gamma_{11}}{\gamma_{11}^2 - \gamma_{12}^2} \times \left[\mu_{1,\alpha_1} + \frac{\gamma_{12}^2}{\gamma_{11}^2} \sum_{\alpha_2} \frac{\mu_{1,\alpha_1}\mu_{2,\alpha_2}}{\mu_{1,\alpha_1} - \mu_{2,\alpha_2}} |\langle 1,\alpha_1 | 2,\alpha_2 \rangle|^2 + O(\gamma_{12}^4) \right], \tag{A9}$$

which always makes the smallest eigenvalue (assumed all positive) get closer to zero, but even in the most dangerous case when this eigenvalue is near marginal, i.e., $\mu_{1,\alpha_1} > 0$ near zero, the second-order correction vanishes as $\mu_{1,\alpha_1} \to 0$. Hence there is no mechanism for it to cross zero. This is not too surprising since the determinant of the matrix in Eq. (A3) cannot change sign as $\gamma_{12}^2 < \gamma_{11}^2$ is increased. Since the eigenvalues remain real (as shown above) they cannot continuously change sign. Hence, as above, we conclude that a stable zero-force fixed point remains stable. Both the size (in phase space) of its basin of attraction (pinned phase) and the Lyapunov exponent may decrease with increasing interlayer coupling, but they do not cross zero.

Finally, note that if e.g., H_1 has a marginal direction, i.e., $H_1 \cdot v^1 = 0$, then $v = (v^1, 0)$ is an eigenvector of M with zero eigenvalue. Hence, a marginal direction remains marginal.

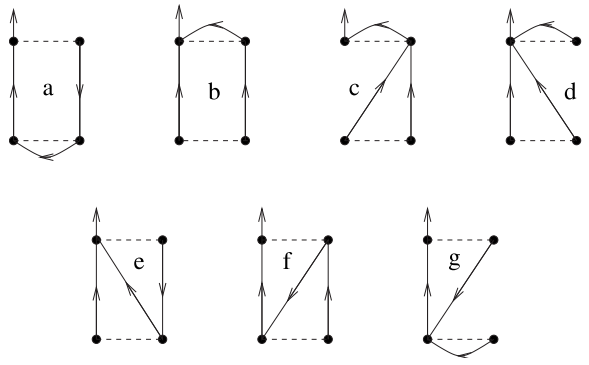

FIG. 20. Two-loop dynamical diagrams correcting the friction. They all have multiplicity 8 except (c) and (d) which have multiplicity 4.

APPENDIX B: TWO-LOOP CALCULATIONS

In this appendix we derive the FRG equations up to two loops using the method of Ref. 18. All calculations are done at zero velocity at the depinning transition. All static quantities like the disorder correlator are the same as for the standard depinning transition, and we refer to Ref. 18 for details. Here we only calculate the corrections to friction, i.e., corrections to γ_{11} and γ_{12}.

1. One-loop order

There are no corrections to γ_{12} at one-loop order since there exists only a single vertex, thus one cannot get a term of the form $\int \tilde{u}^2 \dot{u}^1$. For this, one needs (at least) two loops. Therefore,

$$\delta\gamma_{11}^{1\text{loop}} = -\Delta''(0) I_1 \gamma_{11}, \tag{B1}$$

$$I_1 := \int_p \frac{1}{(p^2 + m^2)^2}. \tag{B2}$$

2. Two-loop order: List of diagrams

There are seven contributions drawn on Fig. 20. Their contribution to γ is symbolically

$$\delta\gamma = -\frac{1}{8} \times 4 \times 2[\mathrm{a} + \mathrm{b} + \mathrm{c} + \mathrm{d} + \mathrm{e} + \mathrm{f} + \mathrm{g}]. \tag{B3}$$

The combinatorial factor is 1/8 from the interaction, 4 from the time ordering of the vertices, and an additional factor of

2 for the symmetry of diagrams a, b, e, f, and g.

The diagrams are calculated as in Ref. 18. When expanding the argument of $\Delta(u^i_{xt}-u^i_{xt'})$, it is important to keep the index of the field. Only diagrams with one disorder on one layer and one disorder on the other layer can give rise to a contribution to γ_{12}, which will be the new feature found below.

3. Expressions for the diagrams

The first combination is

$$\mathrm{a}+\mathrm{g}=-\Delta''(0^+)^2 I_1^2 \tag{B4}$$

as before, since the free integration kills the interlayer term. In the following we give corrections proportional to $\tilde{u}_1$. The index i runs over both layers. Integrations over momenta and time are not written:

$$\mathrm{b}+\mathrm{c}+\mathrm{d}=\tilde{u}_1\sum_i R_{1i}(q_1,t_1)R_{11}(q_2,t_2)R_{1i}(q_1,t_3) \times[|t_3-t_1|-|t_3+t_2-t_1|]\Delta'''(0)\Delta'(0)\dot{u}^i, \tag{B5}$$

$$\mathrm{e}=-\frac{1}{2}\sum_i R_{1i}(q_1,t_1)R_{1i}(q_2,t_2)R_{1i}(q_3,t_3)|t_3-t_2| \times\Delta'''(0)\Delta'(0)\dot{u}^1, \tag{B6}$$

$$\mathrm{f}=-2\Delta'''(0^+)\Delta'(0^+)I_A-2\Delta''(0^+)^2 I_A. \tag{B7}$$

Integrating over times yields the diagrams presented in the next two subsections. They involve the following nontrivial momentum integrals:

$$I_\gamma := \int_{q_1,q_2}\frac{1}{(q_1^2+m^2)(q_2^2+m^2)^2(q_2^2+q_3^2+2m^2)} =\left(\frac{1}{2\epsilon^2}+\frac{1-2\ln 2}{4\epsilon}\right)(\epsilon I_1)^2+\text{finite}, \tag{B8}$$

$$I_A := \int\frac{\mathrm{d}^d q_1}{(2\pi)^d}\frac{\mathrm{d}^d q_2}{(2\pi)^d}\frac{1}{q_1^2+m^2}\frac{1}{q_2^2+m^2}\frac{1}{[(q_1+q_2)^2+m^2]^2} =\left[\frac{1}{2\epsilon^2}+\frac{1}{4\epsilon}+O(\epsilon^2)\right](\epsilon I_1)^2. \tag{B9}$$

They are calculated in Ref. 18.

$$\int_{q_1q_2}\frac{1}{(q_1^2+m^2)(q_2^2+m^2)^2(q_1^2+q_2^2+2m^2)}=\frac{1}{2}I_1^2, \tag{B10}$$

as can be seen by symmetrizing in q_1 and q_2.

4. Corrections to γ_{12}

$$\delta\gamma_{12}^{\mathrm{a+g}}=0, \tag{B11}$$

$$\delta\gamma_{12}^{\mathrm{b+c+d}} =\int_{q_1q_2}\frac{\gamma_{12}^2[(q_1^2+q_2^2)\gamma_{11}^2+(q_2^2-q_1^2)\gamma_{12}^2]\Delta'(0^+)\Delta'''(0^+)}{2q_1^2q_2^2(q_1^2+q_2^2)\gamma_{11}[(q_1^2+q_2^2)^2\gamma_{11}^2-(q_1^2-q_2^2)^2\gamma_{12}^2]}. \tag{B12}$$

In principle, Eq. (B12) should be written with massive propagators. We have put $m=0$ for notational compactness. It is easy to see that for generic values of γ_{11} and γ_{12} Eq. (B12) has no subdivergence for either $q_1\to\infty$ or $q_2\to\infty$, only if they become large together. Properly regularized, it therefore has only a single pole in ϵ, and this pole is universal, i.e., independent of the regularization scheme. For such an integral, which moreover is homogenous in q_1 and q_2, the pole can be expressed as

$$\int_{q_1,q_2} f(q_1^2,q_2^2,m^2)=\frac{(\epsilon I_1)^2}{\epsilon}\int_0^\infty \mathrm{d}(q_2^2) f(1,q_2^2,0)q_2^2+O(\epsilon^0). \tag{B13}$$

This is proven using conformal mappings of the different sectors and was established in Refs. 109–112. Accepting that the integral is indeed universal, a quick way of deriving Eq. (B13) is as follows:

$$\int_{q_1,q_2} f(q_1^2,q_2^2,m^2)\approx\int_{q_1<\Lambda}\int_{q_2} f(q_1^2,q_2^2,0)\approx F\frac{\Lambda^\epsilon}{\epsilon}, \tag{B14}$$

where the "≈" indicates up to terms of $O(\epsilon)$. To obtain the residue F, we derive with respect to Λ, and then set $\Lambda=1$:

$$F\approx S_D\int_{q_2} f(q_1^2=1,q_2^2,0). \tag{B15}$$

Since the integral is finite, we can take the limit of $\epsilon\to 0$ or $d\to 4$. This gives the result Eq. (B13) up to an overall normalization, which is also easily checked.

It is now straightforward to integrate Eq. (B12) using Eq. (B13):

$$\delta\gamma_{12}^{\mathrm{a+b+c}}=\frac{\gamma_{12}\Delta'(0^+)\Delta'''(0)}{4\epsilon}\ln\left|\frac{\gamma_{11}+\gamma_{12}}{\gamma_{11}-\gamma_{12}}\right|. \tag{B16}$$

Note that physically one has to restrict to $\gamma_+>0$ and $\gamma_->0$, thus all results are to be taken in this domain only. The absolute value therefore represents nothing but a notational commodity.

The other two diagrams are trivial:

$$\delta\gamma_{12}^{\mathrm{e}}=0, \tag{B17}$$

$$\delta\gamma_{12}^{\mathrm{f}}=0. \tag{B18}$$

5. Corrections to γ_{11}

Grouping diagrams, which partially cancel, we find for the corrections to γ_{11}:

$$\delta\gamma_{11}^{\mathrm{a+g}}=\gamma_{11}\Delta''(0^+)^2 I_1^2, \tag{B19}$$

$$\delta\gamma_{11}^{\mathrm{b+c+d}} = \int_{q_1 q_2} \frac{[2(q_1^2+q_2^2)^2\gamma_{11}^4 + (-2q_1^4+3q_2^2q_1^2+q_2^4)\gamma_{12}^2\gamma_{11}^2 + q_2^2(q_1^2-q_2^2)\gamma_{12}^4]\Delta'(0^+)\Delta'''(0^+)}{2q_1^2q_2^4(q_1^2+q_2^2)\gamma_{11}[(q_1^2+q_2^2)^2\gamma_{11}^2-(q_1^2-q_2^2)^2\gamma_{12}^2]} \overset{\gamma_{12}=0}{\to} \int_{q_1 q_2} \frac{\gamma_{11}\Delta'(0^+)\Delta'''(0^+)}{q_1^2q_2^4(q_1^2+q_2^2)}. \tag{B20}$$

$\delta\gamma_{11}^{\mathrm{b+c+d}}$ is a little bit more complicated to calculate analytically, since it has a subdivergence, which has to be subtracted if we want to use the magic relation (B13). We observe that subtracting the term at $\gamma_{12}=0$, the diagram has no longer a subdivergence. In order to proceed, one then uses Eq. (B13), and performs a partial fraction decomposition (the variable is q_2^2) of the remaining term, leading to integrals known by Mathematica. The final result is

$$\delta\gamma_{11}^{\mathrm{b+c+d}} = \frac{\gamma_{11}\Delta'(0^+)\Delta'''(0^+)}{2} I_1^2 + \frac{\gamma_{12}\Delta'(0^+)\Delta'''(0^+)}{4\epsilon}\log\left|\frac{\gamma_{11}+\gamma_{12}}{\gamma_{11}-\gamma_{12}}\right|. \tag{B21}$$

The next diagram is

$$\delta\gamma_{11}^{e} = \int_{q_1 q_2} \frac{\gamma_{11}[(q_2^2+q_3^2)^2(q_2^4+q_3^4)\gamma_{11}^2 - (q_2^8-2q_3^2q_2^6-2q_3^4q_2^4-2q_3^6q_2^2+q_3^8)\gamma_{12}^2]\Delta'(0^+)\Delta'''(0^+)}{2q_1^2q_2^4q_3^4(q_2^2+q_3^2)[(q_2^2+q_3^2)^2\gamma_{11}^2-(q_2^2-q_3^2)^2\gamma_{12}^2]}. \tag{B22}$$

We have used the abbreviations $\vec{q}_3 := \vec{q}_1+\vec{q}_2$, and $q_3 := |\vec{q}_3|$. Again, this diagram has a subdivergence (double pole), which we want to subtract. Let us again try the term at $\gamma_{12}\to 0$:

$$\delta\gamma_{11}^{e} \overset{\gamma_{12}\to 0}{\to} \int_{q_1 q_2} \frac{(q_2^4+q_3^4)\gamma_{11}\Delta'(0^+)\Delta'''(0^+)}{2q_1^2q_2^4q_3^4(q_2^2+q_3^2)} = \int_{q_1 q_2} \frac{\gamma_{11}\Delta'(0^+)\Delta'''(0^+)}{q_1^2q_2^4(q_2^2+q_3^2)}. \tag{B23}$$

$\delta\gamma_{11}^{e}$ can be rewritten as

$$\begin{aligned}\delta\gamma_{11}^{e} &= \Delta'(0)\Delta'''(0)\int_{q_1 q_2}\left[\frac{(q_2^4+q_3^4)\gamma_{11}}{2q_1^2q_2^4q_3^4(q_2^2+q_3^2)} + \frac{2\gamma_{11}\gamma_{12}^2}{q_1^2(q_2^2+q_3^2)^3\gamma_{11}^2 - q_1^2(q_2^2-q_3^2)^2(q_2^2+q_3^2)\gamma_{12}^2}\right] \\ &= \Delta'(0)\Delta'''(0)\int_{q_1 q_2}\left\{\frac{\gamma_{11}}{q_1^2q_2^4(q_2^2+q_3^2)} + \frac{2\gamma_{11}\gamma_{12}^2}{q_1^2(q_2^2+q_3^2)[(q_2^2+q_3^2)^2\gamma_{11}^2-(q_2^2-q_3^2)^2\gamma_{12}^2]}\right\}.\end{aligned} \tag{B24}$$

The last integral is

$$\int_{q_1 q_2} \frac{1}{q_1^2(q_2^2+q_3^2)[(q_2^2+q_3^2)^2\gamma_{11}^2-(q_2^2-q_3^2)^2\gamma_{12}^2]} = \frac{\log\left|\frac{\gamma_{11}+\gamma_{12}}{\gamma_{11}-\gamma_{12}}\right|}{4\epsilon\gamma_{11}\gamma_{12}} + \frac{\log\left|1-\frac{\gamma_{12}^2}{\gamma_{11}^2}\right|}{4\epsilon\gamma_{12}^2}. \tag{B25}$$

One way to prove this is as follows. Introduce Schwinger parameters to write the left-hand side of Eq. (B25) as

$$\int_{q_1,q_2}\int_{s_1>0,s_2>0,s_3>0,s_4>0} e^{-s_1(q_2+q_3)^2-(q_2^2+q_3^2)s_2-s_3(\gamma_{11}q_2^2+\gamma_{12}q_2^2+q_3^2\gamma_{11}-q_3^2\gamma_{12})-s_4(\gamma_{11}q_2^2-\gamma_{12}q_2^2+q_3^2\gamma_{11}+q_3^2\gamma_{12})}e^{-s_2}, \tag{B26}$$

where we have introduced a mass for s_2 only (using again universality of the leading pole in ϵ). Then integrate over the q_i's:

$$\int_{s_1>0,s_2>0,s_3>0,s_4>0} e^{-s_2}\{-(s_3-s_4)^2\gamma_{12}^2 + s_2(2s_1+s_2) + (s_3+s_4)\gamma_{11}[2(s_1+s_2)+(s_3+s_4)\gamma_{11}]\}^{-d/2}. \tag{B27}$$

Rescale all s_i with $i\neq 2$ by s_2 and integrate over s_2. Then go to new variables $s_3\to(s+t)/2$, $s_4\to(s-t)/2$. Our integral becomes

$$\int_{s>0}\int_{-s}^{s} dt \int_{s_1>0} \frac{\Gamma(\epsilon)}{2[(s\gamma_{11}+1)(2s_1+s\gamma_{11}+1)-t^2\gamma_{12}^2]^2}. \tag{B28}$$

The result can be simplified to Eq. (B25). A tricky point is logs halfway. Expanding Eq. (B28) in γ_{12}, we circumvent the problem and can check the first terms of the Taylor series. The complete result for $\delta\gamma_{11}^{e}$ is (up to finite terms)

$$\delta\gamma_{11}^{e} = \Delta'(0)\Delta'''(0)\left[\gamma_{11}I_{\gamma} + \frac{\gamma_{12}}{2\epsilon}\log\left|\frac{\gamma_{11}+\gamma_{12}}{\gamma_{11}-\gamma_{12}}\right| + \frac{\gamma_{11}}{2\varepsilon}\log\left|1-\frac{\gamma_{12}^2}{\gamma_{11}^2}\right|\right]. \tag{B29}$$

The final diagram is

$$\delta\gamma_{11}^{f} = \int_{q_1q_2} \frac{\gamma_{11}[(q_1^2+q_2^2)\Delta'(0^+)\Delta'''(0^+)q_3^2 + q_1^2(q_2^2+q_3^2)\Delta''(0)^2]}{q_1^4q_2^4q_3^4} = 2\gamma_{11}\int_{q_1q_2} \frac{\Delta'(0^+)\Delta'''(0^+)+\Delta''(0)^2}{q_1^2q_2^4q_3^2} = 2\gamma_{11}[\Delta'(0^+)\Delta'''(0^+) + \Delta''(0)^2]I_A. \tag{B30}$$

This gives the flow equations given in the main text.

[1] D. S. Fisher, Phys. Rep. **301**, 113 (1998).
[2] S. Ramanathan and D. S. Fisher, Phys. Rev. Lett. **79**, 877 (1997).
[3] S. Ramanathan and D. S. Fisher, Phys. Rev. B **58**, 6026 (1998).
[4] B. Lawn, *Fracture of Brittle Solids*, 2nd ed. (Cambridge University Press, Cambridge, UK, 1993).
[5] G. Blatter, M. V. Feigel'man, V. B. Geshkenbein, A. I. Larkin, and V. M. Vinokur, Rev. Mod. Phys. **66**, 1125 (1994).
[6] T. Giamarchi and S. Bhattacharya, *2001 Cargese School on Trends in High Magnetic Field Science* (Springer-Verlag, Berlin, 2002).
[7] H. Fukuyama and P. A. Lee, Phys. Rev. B **17**, 535 (1978).
[8] G. Gruner, Rev. Mod. Phys. **60**, 1129 (1988).
[9] P. A. Lee and T. M. Rice, Phys. Rev. B **19**, 3970 (1979).
[10] R. E. Thorne, Phys. Today **49** (5), 42 (1996).
[11] A. A. Middleton and D. S. Fisher, Phys. Rev. Lett. **66**, 92 (1991).
[12] A. A. Middleton and D. S. Fisher, Phys. Rev. B **47**, 3530 (1993).
[13] D. S. Fisher, Phys. Rev. B **31**, 1396 (1985).
[14] O. Narayan and D. S. Fisher, Phys. Rev. B **46**, 11520 (1992).
[15] T. Nattermann, S. Stepanow, L. H. Tang, and H. Leschhorn, J. Phys. (France) **2**, 1483 (1992).
[16] P. Chauve, T. Giamarchi, and P. Le Doussal, Phys. Rev. B **62**, 6241 (2000).
[17] P. Chauve, P. Le Doussal, and K. J. Wiese, Phys. Rev. Lett. **86**, 1785 (2001).
[18] P. Le Doussal, K. J. Wiese, and P. Chauve, Phys. Rev. B **66**, 174201 (2002).
[19] P. Le Doussal, K. J. Wiese, and P. Chauve, Phys. Rev. E **69**, 026112 (2004).
[20] A. A. Middleton, Phys. Rev. E **52**, R3337 (1995).
[21] A. Rosso, A. K. Hartmann, and W. Krauth, Phys. Rev. E **67** 021602 (2003).
[22] C. R. Myers and J. P. Sethna, Phys. Rev. B **47**, 11171 (1993).
[23] A. A. Middleton, Phys. Rev. Lett. **68**, 670 (1992).
[24] D. Ertaş and M. Kardar, Phys. Rev. Lett. **73**, 1703 (1994).
[25] D. Ertaş and M. Kardar, Phys. Rev. B **53**, 3520 (1996).
[26] M. Kardar, Phys. Rep. **301**, 85 (1998).
[27] L.-H. Tang, M. Kardar, and D. Dhar, Phys. Rev. Lett. **74**, 920 (1995).
[28] A.-L. Barabasi, G. Grinstein, and M. A. Munoz, Phys. Rev. Lett. **76**, 1481 (1996).
[29] P. Le Doussal and K. J. Wiese, Phys. Rev. E **67**, 016121 (2003).
[30] E. Bouchbinder, M. Bregman, and I. Procaccia, Phys. Rev. E **76**, 025101(R) (2007).
[31] P. Le Doussal, K. J. Wiese, E. Raphael, and R. Golestanian, Phys. Rev. Lett. **96**, 015702 (2006).
[32] E. Katzav, M. Adda-Bedia, M. Ben Amar, and A. Boudaoud, Phys. Rev. E **76**, 051601 (2007).
[33] T. Hwa, Phys. Rev. Lett. **69**, 1552 (1992).
[34] A. E. Koshelev and V. M. Vinokur, Phys. Rev. Lett. **73**, 3580 (1994).
[35] T. Giamarchi and P. Le Doussal, in *Spin Glasses and Random Fields*, edited by A. P. Young (World Scientific, Singapore, 1997); arXiv:cond-mat/9705096 (unpublished).
[36] J. Krug, Phys. Rev. Lett. **75**, 1795 (1995).
[37] L. Balents and M. P. A. Fisher, Phys. Rev. Lett. **75**, 4270 (1995).
[38] T. Giamarchi and P. Le Doussal, Phys. Rev. Lett. **76**, 3408 (1996).
[39] K. Moon, R. T. Scalettar, and G. T. Zimanyi, Phys. Rev. Lett. **77**, 2778 (1996).
[40] L. W. Chen, L. Balents, M. P. A. Fisher, and M. C. Marchetti, Phys. Rev. B **54**, 12798 (1996).
[41] L. Balents, M. C. Marchetti, and L. Radzihovsky, Phys. Rev. Lett. **78**, 751 (1997).
[42] L. Balents, M. C. Marchetti, and L. Radzihovsky, Phys. Rev. B **57**, 7705 (1998).
[43] P. Le Doussal and T. Giamarchi, Phys. Rev. B **57**, 11356 (1998).
[44] F. Pardo, F. de la Cruz, P. L. Gammel, E. Bucher, and D. J. Bishop, Nature (London) **396**, 348 (1998).
[45] P. Chauve, P. Le Doussal, and T. Giamarchi, Phys. Rev. B **61**, R11906 (2000).
[46] E. Olive, J. C. Soret, P. L. Doussal, and T. Giamarchi, Phys. Rev. Lett. **91**, 037005 (2003).
[47] I. S. Aranson, S. Scheidl, and V. M. Vinokur, Phys. Rev. B **58**, 14541 (1998).
[48] S. Scheidl and V. M. Vinokur, Phys. Rev. E **57**, 2574 (1998).
[49] J. M. Schwarz and D. S. Fisher, Phys. Rev. E **67**, 021603 (2003).
[50] S. Bhattacharya and M. J. Higgins, Phys. Rev. Lett. **70**, 2617 (1993).
[51] M. J. Higgins and S. Bhattacharya, Physica C **257**, 232 (1996).
[52] F. Nori, Science **271**, 1373 (1996).
[53] A. Tonomura, Micron **30**, 479 (1999).
[54] H. J. Jensen, A. Brass, Y. Brechet, and A. J. Berlinsky, Phys. Rev. B **38**, 9235 (1988).
[55] M. C. Hellerqvist, D. Ephron, W. R. White, M. R. Beasley, and A. Kapitulnik, Phys. Rev. Lett. **76**, 4022 (1996).
[56] M. C. Hellerqvist, D. Ephron, W. R. White, M. R. Beasley, and

A. Kapitulnik, Phys. Rev. Lett. **77**, 4482 (1996).
[57] W. Henderson, E. Y. Andrei, M. J. Higgins, and S. Bhattacharya, Phys. Rev. Lett. **77**, 2077 (1996).
[58] W. Henderson, E. Y. Andrei, and M. J. Higgins, Phys. Rev. Lett. **81**, 2352 (1998).
[59] D. Pekker, R. Barankov, and P. M. Goldbart, Phys. Rev. Lett. **98**, 175301 (2007).
[60] M. C. Faleski, M. C. Marchetti, and A. A. Middleton, Phys. Rev. B **54**, 12427 (1996).
[61] A. Maeda, M. Notomi, and K. Uchinokura, Phys. Rev. B **42**, 3290 (1990).
[62] R. E. Thorne, K. Cicak, K. O'Neill, and S. G. Lemay, J. Phys. IV **12**, 291 (2002).
[63] S. G. Lemay, M. C. de Lind van Wijngaarden, T. L. Adelman, and R. E. Thorne, Phys. Rev. B **57**, 12781 (1998).
[64] A. M. Troyanovski, J. Aarts, and P. H. Kes, Nature (London) **399**, 665 (1999).
[65] Y. Paltiel, E. Zeldov, Y. N. Myasoedov, H. Shtrikman, S. Bhattacharya, M. J. Higgins, Z. L. Xiao, E. Y. Andrei, P. L. Gammel, and D. J. Bishop, Nature (London) **403**, 398 (2000).
[66] M. Marchevsky, M. J. Higgins, and S. Bhattacharya, Phys. Rev. Lett. **88**, 087002 (2002).
[67] E. Olive and J. C. Soret, Phys. Rev. Lett. **96**, 027002 (2006).
[68] K. E. Bassler, M. Paczuski, and E. Altshuler, Phys. Rev. B **64**, 224517 (2001).
[69] K. E. Bassler and M. Paczuski, Phys. Rev. Lett. **81**, 3761 (1998).
[70] K. E. Bassler, M. Paczuski, and G. F. Reiter, Phys. Rev. Lett. **83**, 3956 (1999).
[71] J. M. Schwarz and D. S. Fisher, Phys. Rev. Lett. **87**, 096107 (2001).
[72] J. M. Schwarz and D. S. Fisher, Phys. Rev. E **67**, 021603 (2003).
[73] A. Montakhab, J. M. Carlson, and J. Levy, Phys. Rev. B **50**, 11227 (1994).
[74] S. H. Strogatz, C. M. Marcus, R. M. Westervelt, and R. E. Mirollo, Phys. Rev. Lett. **61**, 2380 (1988).
[75] S. H. Strogatz and R. M. Westervelt, Phys. Rev. B **40**, 10501 (1989).
[76] V. M. Vinokur and T. Nattermann, Phys. Rev. Lett. **79**, 3471 (1997).
[77] M. C. Marchetti, A. A. Middleton, and T. Prellberg, Phys. Rev. Lett. **85**, 1104 (2000).
[78] M. C. Marchetti and K. A. Dahmen, Phys. Rev. B **66**, 214201 (2002).
[79] K. Saunders, J. M. Schwarz, M. C. Marchetti, and A. A. Middleton, Phys. Rev. B **70**, 024205 (2004).
[80] M. C. Marchetti, A. A. Middleton, K. Saunders, and J. M. Schwarz, Phys. Rev. Lett. **91**, 107002 (2003).
[81] J. Watson and D. S. Fisher, Phys. Rev. B **54**, 938 (1996).
[82] D. Carpentier, P. Le doussal, and T. Giamarchi, Europhys. Lett. **35**, 379 (1996).
[83] J. Kierfeld, T. Nattermann, and T. Hwa, Phys. Rev. B **55**, 626 (1997).
[84] B. Horovitz and P. Le Doussal, Phys. Rev. B **71**, 134202 (2005).
[85] A. Vishwanath and D. Carpentier, Phys. Rev. Lett. **86**, 676 (2001).
[86] M. C. Marchetti, Pramana **64**, 1097 (2005).
[87] M. C. Marchetti, in *Jamming, Yielding, and Irreversible Deformations in Condensed Matter*, edited by M.-C. Miguel and M. Rubi (Springer-Verlag, Berlin, 2006).
[88] A. Pruymboom, P. H. Kes, E. Vanderdrift, and S. Radelaar, Phys. Rev. Lett. **60**, 1430 (1988).
[89] M. H. Theunissen, E. Van der Drift, and P. H. Kes, Phys. Rev. Lett. **77**, 159 (1996).
[90] R. Besseling, R. Niggebrugge, and P. H. Kes, Phys. Rev. Lett. **82**, 3144 (1999).
[91] S. Anders, A. W. Smith, R. Besseling, P. H. Kes, and H. M. Jaeger, Phys. Rev. B **62**, 15195 (2000).
[92] N. Kokubo, R. Besseling, V. M. Vinokur, and P. H. Kes, Phys. Rev. Lett. **88**, 247004 (2002).
[93] T. Nattermann, Phys. Rev. Lett. **64**, 2454 (1990).
[94] D. Cule and T. Hwa, Phys. Rev. Lett. **77**, 278 (1996).
[95] D. Cule and T. Hwa, Phys. Rev. B **57**, 8235 (1998).
[96] T. Giamarchi and P. Le Doussal, Phys. Rev. B **52**, 1242 (1995).
[97] E. Rodriguez-Milla and A. A. Middleton (private communication).
[98] R. Maimon and J. M. Schwarz, Phys. Rev. Lett. **92**, 255502 (2004).
[99] O. Narayan and D. S. Fisher, Phys. Rev. Lett. **68**, 3615 (1992).
[100] T. Nattermann and S. Scheidl, Adv. Phys. **49**, 607 (2000).
[101] J. Levy, M. S. Sherwin, F. F. Abraham, and K. Wiesenfeld, Phys. Rev. Lett. **68**, 2968 (1992).
[102] P. B. Littlewood, Solid State Commun. **65**, 1347 (1988).
[103] L. Balents and P. Le Doussal, Ann. Phys. **315**, 213 (2005).
[104] M. C. Marchetti and K. Saunders, Phys. Rev. B **66**, 224113 (2002).
[105] P. Le Doussal and K. J. Wiese, EPL **77**, 66001 (2007).
[106] T. Emig and T. Nattermann, Phys. Rev. Lett. **79**, 5090 (1997).
[107] A similar static random force is well known to be generated to one loop in the moving phase at $v>0$ (Refs. 36–38, 42, and 43) and would result in a similar effect there. However, it is nontrivial, and only visible at two loops, that such a term also exists at $v=0^+$ at the depinning transition.
[108] Additional effects from KPZ-type terms generated from the partial breakdown of the statistical tilt symmetry (in the relative displacement) will be studied elsewhere.
[109] K. J. Wiese and F. David, Nucl. Phys. B **450**, 495 (1995).
[110] K. J. Wiese, *Ploymerized Membranes, a Review*, Phase Transitions and Critical Phenomena Vol. 19 (Acadamic, London, 1999).
[111] F. David and K. J. Wiese, Phys. Rev. Lett. **76**, 4564 (1996).
[112] K. J. Wiese and F. David, Nucl. Phys. B **487**, 529 (1997).